Regulatory mechanisms for the axonal localization of tau protein in neurons

Minori Iwata[a,†], Shoji Watanabe[a,†,‡], Ayaka Yamane[a], Tomohiro Miyasaka[b,c], and Hiroaki Misonou[a,c,*]
[a]Laboratory of Ion Channel Pathophysiology, Graduate School of Brain Science, [b]Department of Neuropathology, Faculty of Life and Medical Sciences, and [c]Center for Research in Neurodegenerative Diseases, Doshisha University, Kyotanabe-shi, Kyoto 610-0394, Japan

ABSTRACT Tau is a microtubule (MT)-associated protein that is thought to be localized to the axon. However, its precise localization in developing neurons and mechanisms for the axonal localization have not been fully addressed. In this study, we found that the axonal localization of tau in cultured rat hippocampal neurons mainly occur during early neuronal development. Interestingly, transient expression of human tau in very immature neurons, but not in mature neurons, mimicked the developmental localization of endogenous tau to the axon. We therefore were able to establish an experimental model, in which exogenously expressed tau can be properly localized to the axon. Using this model, we obtained a surprising finding that the axonal localization of tau did not require stable MT binding. Tau lacking the MT-binding domain (MTBD) exhibited high diffusivity but localized properly to the axon. In contrast, a dephosphorylation-mimetic mutant of the proline-rich region 2 showed reinforced MT binding and mislocalization. Our results suggest that tight binding to MTs prevents tau from entering the axon and results in mislocalization in the soma and dendrites when expressed in mature neurons. This study therefore provides a novel mechanism independent of MTBD for the axonal localization of tau.

INTRODUCTION

Tau is a microtubule (MT)-associated protein (MAP) that is thought to be localized in the axon of a neuron in normal physiological conditions (Binder *et al.*, 1985; Peng *et al.*, 1986; Brion *et al.*, 1988; Migheli *et al.*, 1988; Trojanowski *et al.*, 1989). We have recently developed new anti-tau antibodies that are sensitive enough to detect unaggregated tau in brain tissues and demonstrated the precise axonal localization of tau in the mouse brain unambiguously (Kubo *et al.*, 2019a). In contrast, in Alzheimer's disease (AD) and related disorders, tau mislocalizes to the soma and dendrites, where tau ultimately forms neurofibrillary tangles (Attems and Kurt, 2013). Understanding this mislocalization is a key to understand the pathogenesis of AD, as tau pathology is unambiguously linked to neurodegeneration from pathological and genetic evidence (Gómez-Isla *et al.*, 1997; Delacourte *et al.*, 1999; Ghetti *et al.*, 2015). Also, this mislocalization may be a prerequisite for tau to cause synaptic dysfunction, which has been recently proposed as an early pathological step before tangle formation and neurodegeneration (Decker *et al.*, 2015). Understanding how normal or physiological tau is localized to and maintained in the axon would help us to gain insights into how these mechanisms are impaired.

Previous studies have made considerable efforts to study and understand the mechanisms for the axonal localization of tau. These studies have revealed essentially two major mechanisms. First, tau is transported to the axon by MT- and motor protein–based mechanisms (Utton *et al.*, 2005; Falzone *et al.*, 2009; Scholz and Mandelkow, 2014). Second, a MT-based filter situated near or in the axon initial segment restricts tau from entering the soma while allowing it to go into the axon (Li *et al.*, 2011). However, one big challenge remaining in studying these mechanisms is to localize exogenous
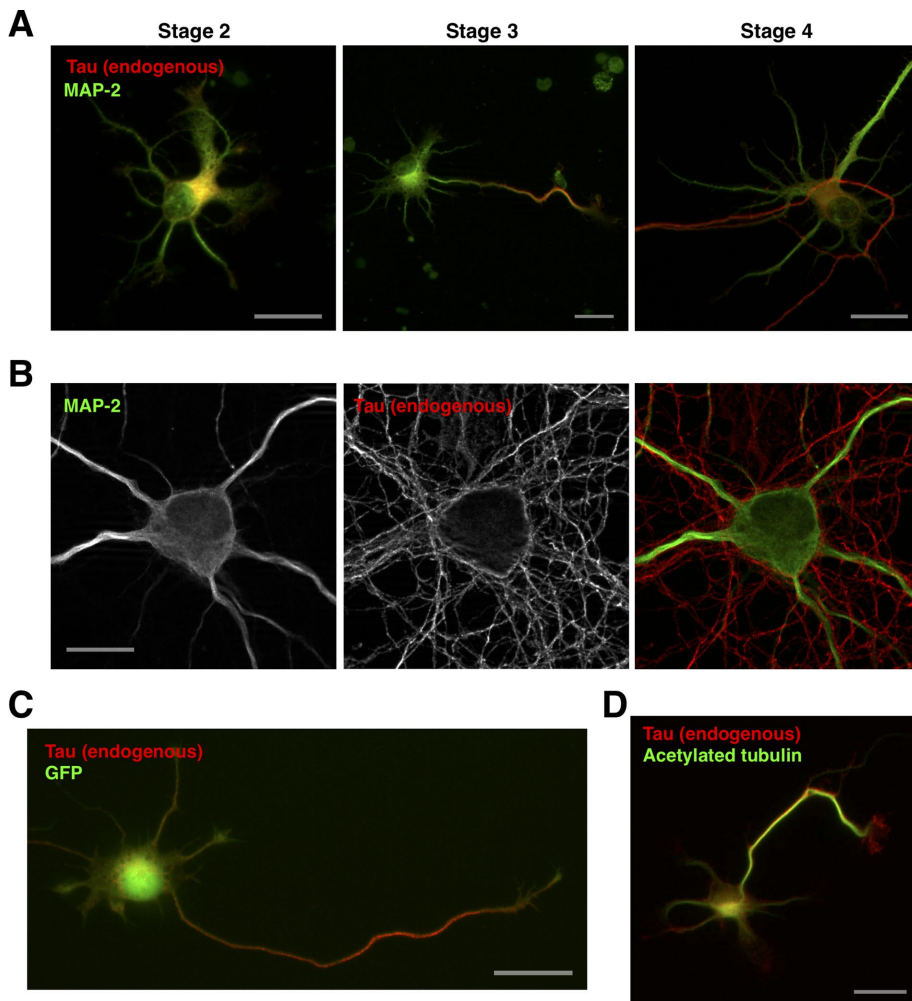
FIGURE 1: Subcellular distribution of endogenous tau in developing neurons in culture. (A) Distribution of endogenous tau in stage 2, 3, and 4 neurons. Neurons were immunostained for endogenous tau (RTM38) and MAP-2. Scale bars, 20 μm. (B) Axonal localization of endogenous tau in mature neurons at 16 DIV immunostained for MAP-2 (green) and tau (red) with RTM38. Scale bars, 20 μm. (C) Distributions of endogenous tau and GFP expressed in stage 3 neurons at 3 DIV. Scale bar, 20 μm. (D) Distributions of endogenous tau and acetylated tubulins in stage 3 neurons. Scale bar, 20 μm.

tau is expressed like endogenous tau and colocalizes with endogenous tau in the axon in both developing and matured neurons. With this model, we show novel findings on the relationship between MT binding and axonal localization of tau, the involvement of the proline-rich region in tau localization, and how phosphorylation affects the localization and MT binding. These results would provide new questions and hypotheses regarding how tau localizes to the axon and how it is disrupted in AD.

RESULTS

Axonal localization of total tau in neurons

The tau-1 antibody has been widely used to label the axons, as dephosphorylated tau at Ser-195, Ser-198, Ser-199, and Ser-202 (Szendrei *et al.*, 1993) has been shown to highly accumulate in the axons of immature neurons in culture (Mandell and Banker, 1996). Although total tau has also been shown to be accumulated in distal axons (Mandell and Banker, 1996), its precise subcellular localization has not been extensively studied. Using antibodies we recently developed (Kubo *et al.*, 2019a), which can detect unaggregated tau at high sensitivity and independently of phosphorylation, we confirmed that total endogenous tau is highly accumulated in distal axons even in stage 3 neurons in 2–3 DIV (days in vitro) cultures (Figure 1A). This became more pronounced in stage 4 neurons in 4–5 DIV cultures, and tau is restricted to the axon in mature neurons by 16 DIV (Figure 1B). The axonal accumulation in stage 3 neurons is not due to the increasing volume of the distal axon, as GFP did not exhibit such accumulation (Figure 1C). Also, acetylated tubulin, which has also been shown to be accumulated in distal axons in immature neurons (Hammond *et al.*, 2010), colocalized with tau at a high degree. These results suggest that the axonal localization process of tau starts already in stage 3 neurons.

A new experimental system in which exogenous tau is localized to the axon

To study the mechanism of the axonal localization of tau, researchers have used cultured neurons to express exogenous tau with a tag, such as GFP. Typically, cultured neurons are transfected at 5–10 DIV, when they are most transfection competent, and tau expression is induced constitutively by a strong promoter such as a cytomegalovirus (CMV) promoter. However, expressed tau with a promoter like CMV is scarce in the axon but highly accumulated in the soma and dendrites (Figure 2A), such that one cannot use this kind of experimental system to study the precise localization mechanisms. This is not due to extreme overexpression of exogenous tau, as we observed only a marginal increase of immunoreactivity to our antibody (Figure 2B), which detects rodent and human tau at similar sensitivities on Western blotting (Kubo *et al.*, 2019a). We therefore

tau to the axon, where endogenous tau localizes. When tau is constitutively expressed in cultured neurons by transfection, it typically distributes uniformly throughout the cells (Xia *et al.*, 2016), such that the major population of tau remains in the soma and dendrites (see Figure 2A later in the article). This "mislocalization" makes it difficult to study axonal localization mechanisms of tau in a precise manner. We therefore set to tackle this challenge and establish a good experimental model for studying tau localization.

We have recently showed that tau mRNA expression is high during the first week of postnatal development in mice (Kubo *et al.*, 2019b). We also demonstrated that expressing human tau in the same manner as endogenous tau results in its axonal localization in knock-in mice, whereas human tau expressed beyond the developmental period mislocalizes to the soma and dendrites in tau transgenic mice (Kubo *et al.*, 2019b). In this article, we show that this holds true in cultured neurons, such that exogenous human tau can be localized to the axon, only when it is expressed early during neuronal development. Using an inducible expression system, we were able to establish an experimental model in which exogenous
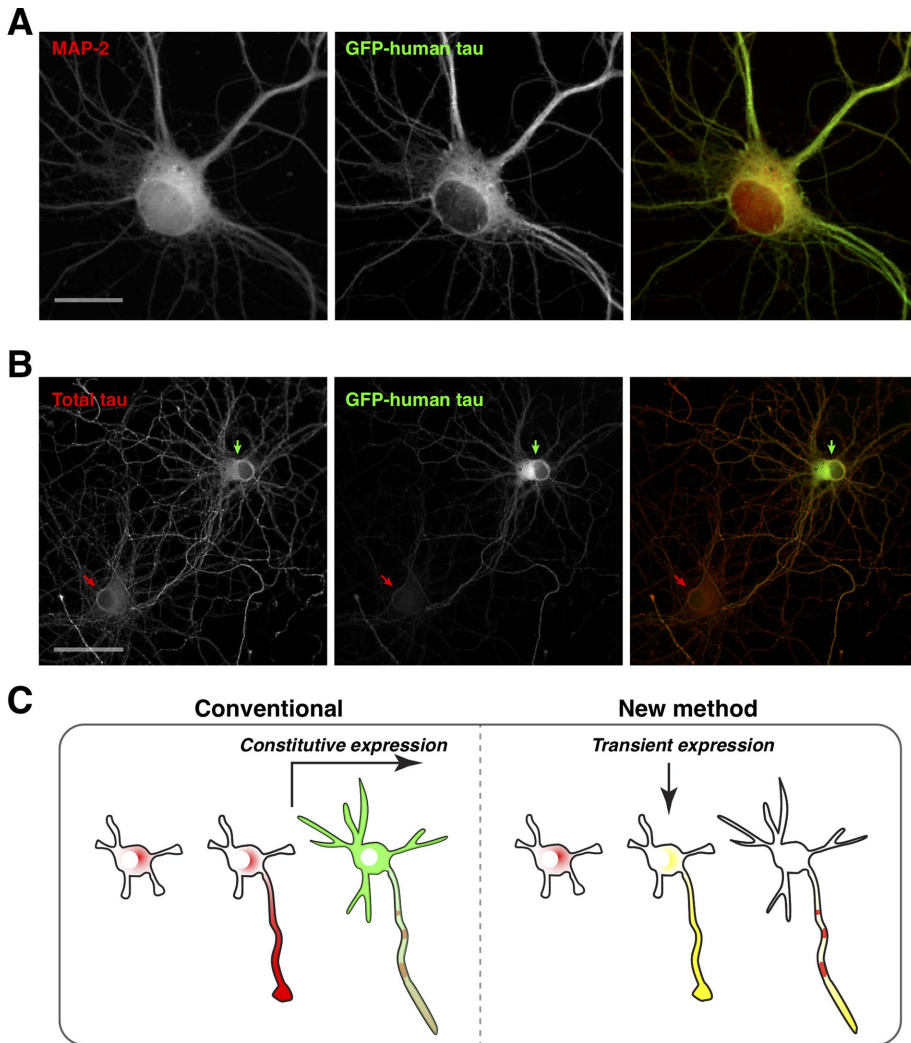
FIGURE 2: Mislocalization of exogenously expressed tau. (A) Mislocalization of exogenous human tau tagged with GFP (green). Neurons were transfected with GFP-tau at 7 DIV, fixed, and immunostained for MAP-2 (red) at 14 DIV. Scale bar, 20 μm. (B) Expression levels of exogenous tau in transfected neurons. Neurons were transfected with GFP-tau at 7 DIV, fixed, and immunostained for total tau with RTM38 at 9 DIV. Transfected and untransfected neurons are indicated with green and red arrows, respectively. Scale bar, 50 μm. (C) Scheme illustrating our method. Red and green indicate endogenous and exogenous tau, respectively. Endogenous tau (red) is expressed in stage 2 neurons and becomes preferentially distributed in the axon in stage 3 neurons. In conventional methods, exogenous tau (green) is expressed constitutively beyond this stage and mislocalizes to the soma and dendrites. In our new method, the expression of exogenous tau is induced in immature neurons around stages 2 and 3 only transiently. This would result in axonal localization of exogenous tau.

To test this, we constructed Tet-ON lenti-viral vectors, with which the expression of exogenous tau can be controlled pharmacologically via the tetracycline transactivator (Urlinger *et al.*, 2000). Cultured neurons were infected with lentiviral particles at 0 DIV (at the day of plating) and treated with doxycyclin to induce the expression for 1 h at 1 DIV. Using this system, we were able to recapitulate the developmental localization of tau, such that human tau was concentrated in the distal axon and colocalized with endogenous tau in stage 3 neurons (Figure 3, A and C). Direct fluorescence imaging of GFP-tau in living neurons also exhibited the preferential distribution of tau in the axon (Figure 3B). We quantified the fluorescence signals and compared the axon/dendrite ratios between endogenous and exogenous tau (Figure 3D). They showed comparable ratios in each cell and were not statistically different. Although the expression was induced only for 1 h, GFP-tau was readily detected even in 14 DIV neurons, indicating that the turnover of tau is slow as previously implicated (Mercken *et al.*, 1995; Morales-Corraliza *et al.*, 2009; Yamada *et al.*, 2015; Sato *et al.*, 2018). Importantly, exogenous tau maintained the axonal colocalization with endogenous tau in 14 DIV neurons, while it was virtually absent from MAP-2–positive dendrites (Figure 3, E and F). These results demonstrate a novel experimental system, in which exogenous tau is properly localized to the axon with endogenous tau in developing neurons.

We then tested whether it is the timing and/or the briefness of the expression required for the proper localization. Exogenous tau expressed constitutively from 1 DIV did not localize preferentially to the axon, indicating that it is the transient expression (unpublished data). We therefore expressed human tau at 7 DIV for 1 h to investigate the importance of the timing. In contrast to human tau expressed at 1 DIV (Figure 3E), that expressed at 7 DIV remained in the soma and dendrites, and was detected only at low

sought to address this issue and to establish an experimental system in which exogenous tau localizes to the axon. We have recently reported that the expression of endogenous tau is at the highest during the perinatal period and greatly reduced during the first couple of weeks after birth (Kubo *et al.*, 2019b). The axonal localization of endogenous tau occurs early at day 7 after birth and is completed by day 14. We also showed that exogenous human tau expressed in the same manner as endogenous tau using the knock-in method localizes properly to the axon, while human tau expressed under an ectopic promoter mislocalizes to the soma and dendrites (Kubo *et al.*, 2019b). On the basis of these observations, we hypothesized that for exogenous tau to be properly localized to the axon it needs to be expressed transiently during early development (Figure 2C).

levels in the axons (Figure 4, A and B). To compare the difference, we computed the axon/dendrite ratio (see *Materials and Methods*) of exogenous tau and normalized it to that of endogenous tau in each neuron, such that similar localization would result in a value close to 1. As shown in Figure 4C, human tau expressed at 1 DIV exhibited a mean value close to 1 as expected. However, it became significantly low when tau was expressed transiently at 7 DIV, showing that exogenous tau is mislocalized in these neurons. These results indicate that tau needs to be expressed early and transiently like endogenous tau to localize properly to the axon.

This notion was also supported by results from animal models. Using our rodent and human tau–specific antibodies (Kubo *et al.*, 2019a), we can demonstrate that, in human tau transgenic mice,
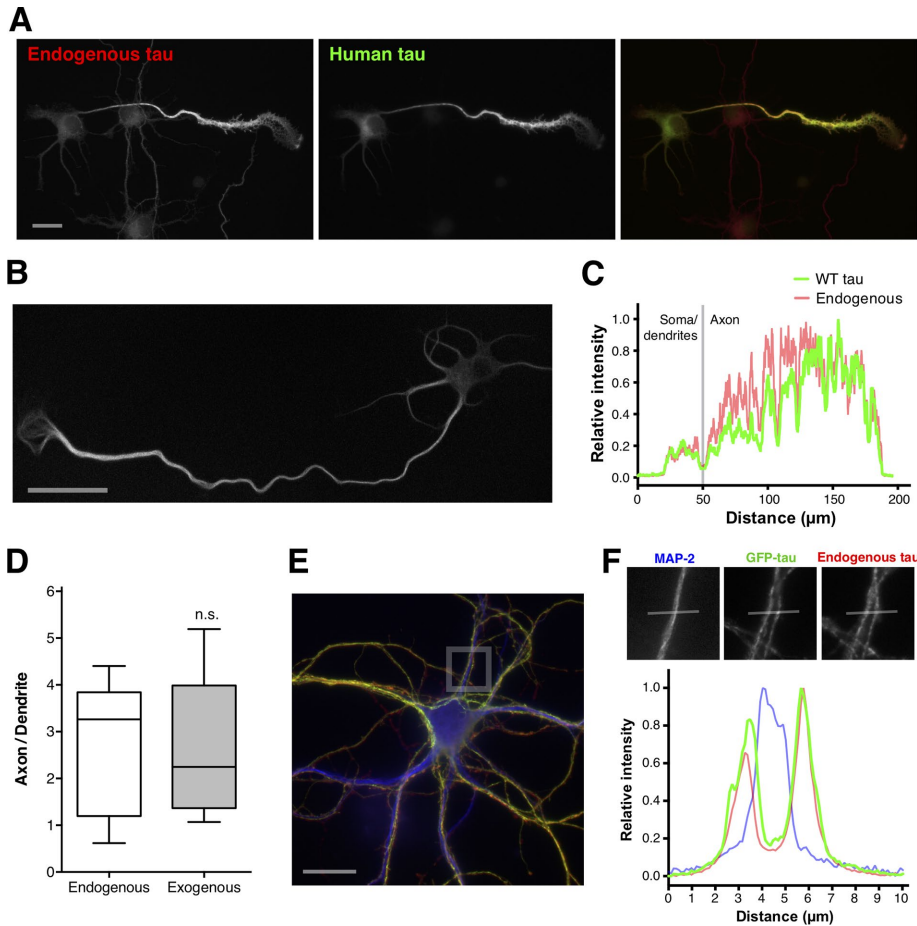
FIGURE 3: Normal axonal localization of exogenous tau by following the expression profile of endogenous tau. (A) Axonal localization of exogenous human tau using the new method. Neurons were infected with lentivirus encoding GFP-tagged human tau at 1 DIV, treated with doxycycline at 1 µg/ml for 1 h, fixed at 3 DIV, and immunostained for endogenous tau (red with rodent tauN) and GFP (green). Scale bar, 20 µm. (B) Distribution of GFP-tagged tau in neurons at 3 DIV. Direct fluorescence signals from GFP are shown. Scale bar, 20 µm. (C) Line scan analysis of endogenous tau (red) and human tau (green) of the neuron shown in A. The vertical gray line indicates the border between the soma and the axon. (D) Quantification of the ratio of axonal signals over dendritic signals for endogenous and human tau in 3 DIV neurons. There was no significant difference between them (n.s., $p = 0.92$ using a Wilcoxson matched-pairs signed rank test, $n = 10$). (E) Triple immunolabeling of neurons, in which the expression of GFP-tagged tau (GFP-tau) was induced at 1 DIV, for GFP-tau (green, anti-GFP), endogenous tau (red, rodent tauN), and MAP-2 (blue) at 14 DIV. Scale bar, 20 µm. (F) Line scan analysis of endogenous tau (red), GFP-tau (green), and MAP-2 (blue) in the neuron shown in E. Top panels show high-magnification images of the area indicated in E, which were used for the analysis.

knockout mice. Exogenous tau was distributed not only to the axon but also in the soma and dendrites (Figure 4, F and G). Also, P301L human tau was mislocalized to the somata and dendrites, even when it is expressed in tau knockout mice as a transgene (Figure 4H). These results suggest that the mislocalization of exogenous human tau does not result from the competition with endogenous tau.

We then considered whether the MT binding of tau differs between young and mature neurons, as MT binding has been implicated as an integral part of axonal localization of tau (Scholz and Mandelkow, 2014). To test this, we performed the fluorescence recovery after photobleaching (FRAP) experiments to measure the mobility of GFP-tau and assume in situ MT binding. Diffusional motion and MT binding of tau have been studied in neurons using FRAP and single-molecule tracking techniques (Konzack *et al.*, 2007; Weissmann *et al.*, 2009; Janning *et al.*, 2014; Tortosa *et al.*, 2017). In our experimental system, we observed somewhat slow mobility of GFP-tau in distal axons in neurons at 3 DIV (Figures 5A and 4B) with the half-time of recovery at ~15 s. We fitted the recovery phase with a one-dimensional diffusion model (Ellenberg and Lippincott-Schwartz, 1999) and obtained the diffusion coefficient of 0.15 ± 0.01 µm^2/s (Figure 5B), which is much smaller than that previously reported. This mobility in the axon became slower during the maturation of neurons, such that there were small but significant differences in FRAP at 3, 7, and 14 DIV (Figure 5C). In contrast, the mobility of GFP-tau in the soma changed substantially and was significantly decreased between 3 and 14 DIV (Figure 5, D and E).

To verify whether the mobility of GFP-tau reflects its MT binding in situ, we examined the effect of a MT depolymerizing agent, nocodazole, on GFP-tau FRAP. We found that nocodazole treatment resulted in the accel-

exogenous human tau with the P301L mutation, which is expressed under the regulation of the CaMKII promoter, mislocalizes to the somata and dendrites unlike endogenous tau in the same neurons (Figure 4D). The mislocalization of human tau is not due to the mutation because it can properly localize to the axon in knock-in mice, in which the P301L human tau is expressed by the endogenous tau promoter (Figure 4E). These results suggest that for exogenous tau to be localized to the axon it needs to be expressed like endogenous tau.

MT binding and axonal localization of tau

We then investigated what makes tau mislocalize when expressed in mature neurons. First, we considered the competition between endogenous and exogenous tau. To test this, human tau was expressed for 1 h at 7 DIV in cultured neurons prepared from tau

eration of FRAP (Figure 5F) with significant increases in the plateau (Figure 5G) and slope (Figure 5H), when data were fitted with exponential functions (see *Materials and Methods*). To further validate the FRAP assay, we also generated tau lacking the MT-binding domain (MTBD; Figure 6A) and tested it in an in vitro MT-binding assay (Figure 6B) and in FRAP in neurons. As expected, recombinant tau lacking MTBD (tau ΔMTBD) purified from *Escherichia coli* exhibited significantly reduced MT binding ($p < 0.0001$ with $q (30) = 7.145$ using analysis of variance (ANOVA) with Dunnett's test; analysis done altogether with all the mutants as shown in Table 1), whereas wild-type tau (WT tau) was detected mostly in the MT-bound fraction (Figure 6C; see also Table 1 for details). We then performed FRAP in the axons of cultured neurons. As shown in Figure 6D, in contrast to the slow recovery of WT tau, GFP-tagged ΔMTBD showed a virtually complete and faster recovery, indicating that ΔMTBD diffuses almost

freely. When the normalized fluorescence signals were fitted with single exponential functions (Figure 6E), the slopes and the immobile fraction differ significantly between WT tau and tau ΔMTBD (Table 2). These results demonstrate that the molecular mobility of tau measured in FRAP reflects its MT binding in situ.

To test whether the facilitated MT binding in mature neurons prevents exogenous tau from exiting the soma, we also generated a mutant that shows facilitated MT binding in situ. Because the proline-rich region 2 contains several phosphorylation sites that are known to be hyperphosphorylated in neurons in AD patients, and has been shown to participate in MT binding (Kiris *et al.*, 2011; Schwalbe *et al.*, 2015), we generated tau, of which all eight putative phosphorylation sites in PRR2 (Figure 7A) are replaced with alanine (Tau PRR2_Ala) to mimic dephosphorylation in a similar but more restricted way to the previous study (Rodríguez-Martín *et al.*, 2013). It should be noted that four phosphorylation sites (Ser-195, Ser-198, Ser-199, and Ser-202) are the putative epitope of the tau-1 antibody. In the biochemical assay, PRR2_Ala was found only in the bound fraction and indistinguishable from WT (Figure 7B). This is presumably because recombinant WT tau is completely dephosphorylated and therefore behaves like recombinant PRR2_Ala. Surprisingly, tau PRR2_Ala showed a dramatic reduction in FRAP (Figure 7, C and D) with a significantly reduced slope compared with WT (Table 2). These results suggest that phosphorylation of PRR2 strongly regulates MT binding of tau in neurons (see below for deletion), and that PRR2_Ala exhibits facilitated MT binding in axons.

We then analyzed their localizations. Surprisingly, ΔMTBD did localize to the axon like WT tau in stage 3 neurons at 3 DIV (Figure 7E) and in more mature neurons at 7 DIV (Figure 7F). This was very surprising from its diffusive nature (Figure 6) and literature reporting the importance of MTBD in the axonal localization and transport of tau (Kanai and Hirokawa, 1995; Utton *et al.*, 2005; Falzone *et al.*, 2009; Weissmann *et al.*, 2009; Li *et al.*, 2011; Scholz and Mandelkow, 2014). In contrast, PRR2_Ala was highly retained in the soma and dendrites at 3 DIV (Figure 7E) and 7 DIV (Figure 7F). Their differences can be readily appreciated in the line scan analyses at 3 DIV (Figure 7, G and H) and by the significant difference in the axon/dendrite ratios (Figure 7I). The axonal localization of ΔMTBD was stable into mature neurons and comparable to that of endogenous tau at 14 DIV (Figure 8, A and B). These results suggest that MT binding is rather preventive for the axonal localization of tau. As shown earlier in Figure 5, we found that MT binding appears to be facilitated in the soma in mature neurons as compared with immature neurons. Therefore, we hypothesized that this facilitated MT binding prevents tau from efficiently localizing to the axon in mature neurons. To test this, we induced the expression of WT tau or ΔMTBD at 7 DIV for 1 h and analyzed their localizations at 14 DIV. WT tau was readily detectable in the soma and dendrites positive for MAP-2 (Figure 8C). In contrast, ΔMTBD was highly colocalized with endogenous tau in the axons (Figure 8C) and indistinguishable from WT tau (Figure 3E) and ΔMTBD expressed at 1 DIV (Figure 8A). The axon/dendrite ratios also support their high degree of colocalization in the axons and was significantly different from those of WT tau (Figure 8D). Taken together, these results suggest that MT binding regulated by the phosphorylation state of PRR2 strongly influences the ability of tau to localize to the axon during neuronal development.

Localization mechanisms of tau
Our data suggest that MTBD and stable MT binding are not necessary for the axonal localization of tau. We therefore sought to investigate how tau localizes to the axon without these properties. We considered three plausible mechanisms for tau to localize to the axon (Figure 9A). One obvious mechanism was that axonal MTs trap tau in the axon. However, we rejected this model because ΔMTBD was diffusible anywhere in neurons; even near the tip of the axon, where it is highly accumulated (Figure 9, B and C). The diffusivity was also comparable in dendrites and the axon (Figure 9D). Also, its high diffusivity indicates that a large portion of ΔMTBD does not bind to any large structures, such as actin filaments and neurofilaments. Therefore, we sought to test the alternative models.

It has been proposed that the axon initial segment functions as a size filter for cytoplasmic proteins and organelles (Song *et al.*, 2009). Mandelkow and colleagues have also proposed that there is a filter or barrier that allows the entrance of tau into the axon but prevents it from returning to the soma (Li *et al.*, 2011). To test whether there is a barrier/filter like this, we performed FRAP of ΔMTBD in the soma. Neurons expressing ΔMTBD at 3DIV (Figure 9E) were subjected to somatic FRAP. We expected that there was no significant recovery of ΔMTBD in the soma, as axonal ΔMTBD would not reenter the soma. However, when the entire somatodendritic region was photobleached as shown in Figure 9E, there was a rapid and substantial recovery of the somatodendritic fluorescence as well as a concomitant decrease of the axonal fluorescence (Figure 9F). This suggests that tau ΔMTBD is freely diffusible from the axon to the soma and dendrites, in spite of its overall axonal localization. These results do not support the barrier/filter model.

We next examined the directional transport of tau to the axon using FRAP. GFP-tagged WT tau was photobleached in the beginning part of the axon as shown in Figure 9G. This allowed us to monitor the flow of fluorescent molecules from proximal and distal sides and to test whether there is a directional bias. We found that WT tau exhibited an asymmetric flow after photobleaching, such that the fluorescence signal recovered preferentially from the somatic side of the bleached area (Figure 9G). This can be visualized using a kymograph (Figure 9H) and line scans at different time points (Figure 9I). We also measured fluorescence recovery at the proximal and distal ends of the bleached area. As expected from the biased recovery, we found a significantly faster recovery in the proximal end than in the distal end (Figure 9J).

To further test whether there is axon-biased movement of tau from the soma, we employed a pulse-chase strategy with a photoconvertible protein, Dendra2, tagged with WT tau. Dendra2-tau was expressed at 1 DIV for 1 h and exhibited axonal accumulation like GFP-tagged WT tau (unpublished data). Photoconversion was performed in the soma, and changes in the distribution were analyzed in time-lapse images. We focused on the axon and a dendrite, which were adjacent and have similar distances from the photoconversion spot, in each cell. A line was drawn over the axon and the dendrite to measure fluorescence intensities after photoconversion (Figure 10A). As we expected, converted Dendra2-tau spread more readily to the axon than to the dendrite (Figure 10B). We divided the curves at the center to the axonal and dendritic sides and measured the area under the curve at 20 s after photoconversion (Figure 10B). The result showed that the area was significantly greater ($p = 0.0292$ using a paired t test) for the axonal side than for the dendritic side (Figure 10C), indicating that tau distributes to the axon faster than to the adjacent dendrite. These results from FRAP and photoconversion suggest that there is a transport mechanism delivering tau to the axon.

Axonal localization mediated by the PRR2
Because the deletion of MTBD did not affect the localization of tau, we aimed to determine the region of tau determining its axonal
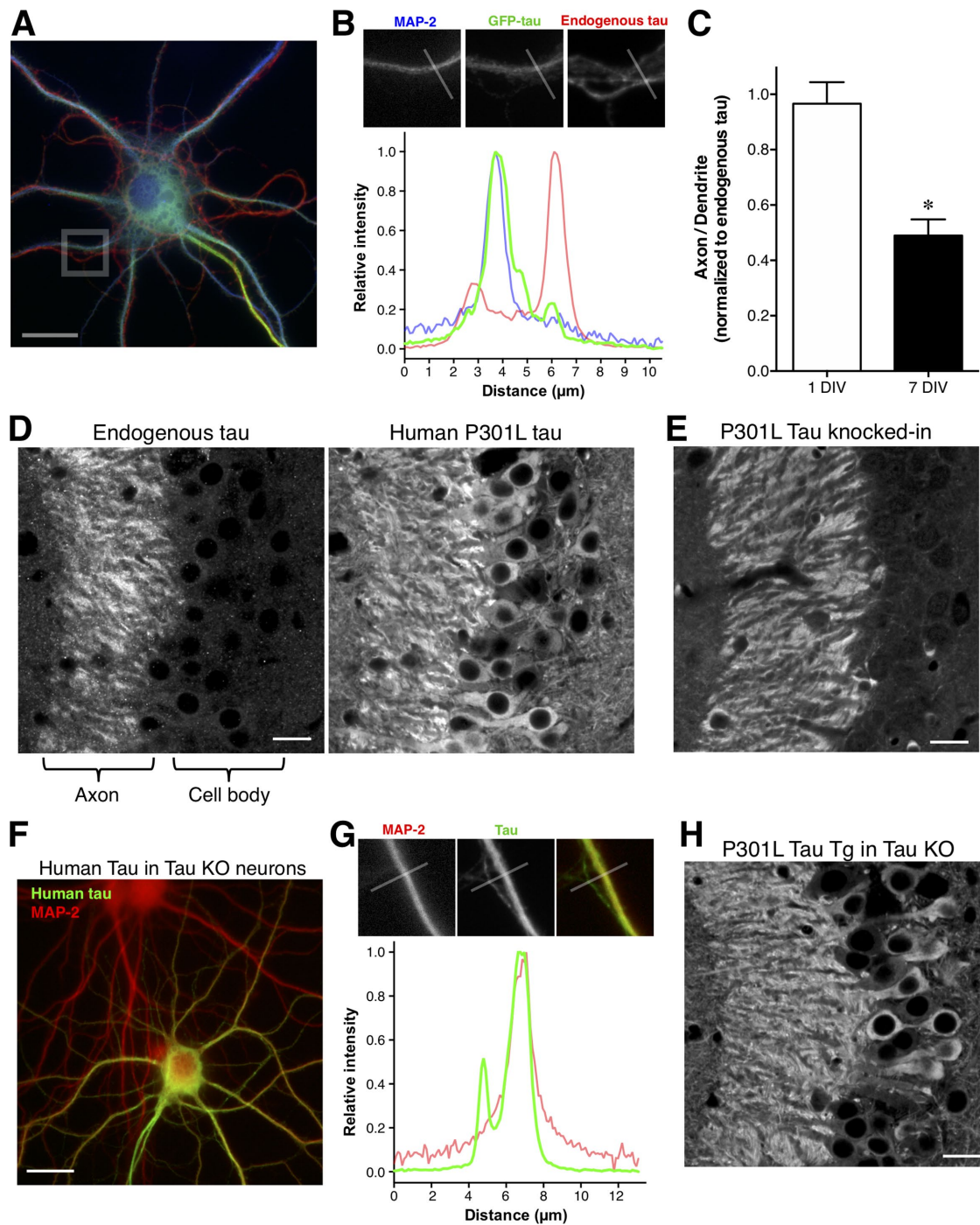
FIGURE 4: Axonal localization of tau determined by the timing of expression. (A) Triple immunolabeling of neurons, in which the expression of GFP-tau was induced for 1 h at 7 DIV, for GFP-tau (anti-GFP), endogenous tau (rodent tau N), and MAP-2 at 14 DIV. Scale bar, 20 μm (right). (B) Line scan analysis of endogenous tau (red), GFP-tau (green), and MAP-2 (blue) in the neuron shown in A. Top panels show high-magnification images of the area indicated in A that were used for the analysis. (C) Colocalization of exogenous tau with endogenous tau in the axon only when expressed in young neurons. We analyzed how exogenous tau is enriched in the axon like endogenous tau by quantifying the ratio of axonal signals over dendritic signals normalized to those of endogenous tau. Note that a good overlap of them would provide a value close to 1. *, $p = 0.0079$ using a Mann-Whitney test ($n = 5$). (D) Mislocalization of human tau with the P301L mutation in the hippocampus of human tau transgenic mice, in which the expression is driven by the calcium/calmodulin kinase II promotor. The CA3 region of the hippocampus was immunolabeled for endogenous mouse tau (rodent tauN) and human tau (tau12). While endogenous tau was detected only in the stratum lucidum in the mossy fiber axons, human tau was detected both in the axons and the somata of CA3 pyramidal neurons. Scale bar, 20 μm. (E) Proper axonal localization of P301L tau in the hippocampus of human tau knock-in mice. Scale bar, 20 μm. (F) Mislocalization of human WT tau in neurons prepared from tau knockout mice. Neurons were treated with doxycycline at 7 DIV, fixed, and immunostained for MAP-2 (red) and human tau (green, anti-GFP)) at 14 DIV. Similar to

localization using a series of deletion mutants. We found that removing the PRR2 (ΔPRR2; see Figure 6A) caused a drastic effect on MT binding and localization. First, the biochemical MT-binding assay revealed that ΔPRR2 exhibits a significant albeit slight loss of MT binding ($p = 0.0295$ with q (30) = 2.887; Figure 11, A and B, and Table 1). Interestingly, deletion of both PRR2 and MTBD resulted in a greater reduction of MT binding than ΔMTBD and almost complete loss of MT binding ($p < 0.0001$ with q (30) = 17.95 against WT; Figure 11, A and B, and Table 1). FRAP analyses of ΔPRR2 also showed significant increases in the recovery rate (0.075 ± 0.004 vs. 0.1389 ± 0.0157, $p = 0.0087$) and the mobile fraction (0.6307 ± 0.0234 vs. 0.7814 ± 0.0235, $p = 0.0011$) compared with WT tau (Figure 11C and Table 2), suggesting that PRR2 participates in MT binding as previously indicated (Butner and Kirschner, 1991; Gustke et al., 1994; Goode et al., 1997).

As shown in Figure 10C, ΔPRR2 was retained in the soma in stage 3 neurons at 3 DIV, while WT tau was preferentially distributed to the axon. Double immunolabeling of ΔPRR2 and endogenous tau also showed that ΔPRR2 localization was dramatically different from that of endogenous tau (Figure 11D). This difference was also evidenced by the line scan analysis of fluorescence signals (Figure 11D). Mislocalization of ΔPRR2 occurred in the absence of endogenous tau in tau knockout neurons (unpublished data). We also compared the axon/dendrite ratios and confirmed that ΔPRR2 tau showed a significantly smaller ratio (0.9069 ± 0.1478 vs. 0.4851 ± 0.0675, $p = 0.0199$, q (28) = 2.989, ANOVA with Dunnett's post hoc test, analysis done altogether with all the mutants as shown in Table 3) than WT tau, showing that it is not enriched in the axon. This mislocalization was maintained in more mature neurons as shown in Figure 11E, such that ΔPRR2 was present in the soma and dendrites as well as the axons (Figure 11F). This was also reflected in the reduced axon/dendrite ratio (Figure 11G). These results suggest that PRR2 is critical for the axonal localization of tau.

We next sought to examine whether the PRR2 domain is also involved in the directional transport of tau to the axon using FRAP. While WT tau exhibited an asymmetric flow after photobleaching, ΔPRR2 exhibited more symmetric recovery (Figure 12A). To better quantify this difference, we performed FRAP in the axon where the thickness and fluorescence signals are comparable (Figure 12B). The recovery was monitored using a line profile function and plotted against the distance. As shown in the line graphs, the recovery was asymmetric for WT tau but not for ΔPRR2. We measured the area under the curve in the proximal and distal bleached areas as indicated in Figure 12C. This showed that the recovery was significantly greater ($p = 0.0012$ with t (4) = 9.841 using repeated measures two-way ANOVA with Sidak's post hoc tests, $n = 3$) in the proximal side of the bleached area than the distal side for WT tau, whereas no significant difference was observed for ΔPRR2 ($p = 0.7280$). Taken together, these results suggest that PRR2 is necessary for the axonal localization of tau and the directional transport of tau to the axon.

DISCUSSION

In this article, we demonstrated a new cellular model to study the mechanisms for the axonal localization of tau. We first established that bulk of tau rapidly localizes to the axon in developing neurons

in culture using our sensitive and specific antibodies. We then established a method to recapitulate this developmental localization with exogenously expressed tau, such as GFP-tagged human tau. Our experimental model is unique and different from previously used culture models, in which exogenous tau is constitutively expressed and distributes throughout the cell. Therefore, we believe that our experimental system provides a new platform to study the mechanisms of tau localization and mislocalization.

Axonal localization dictated by the timing of tau expression

The key to establish the model was to express tau in immature neurons for a short period of time. Both the timing and the briefness of expression were critical to realize proper axonal localization of exogenous tau in neurons. When tau expression was induced for 1 h at 1 DIV, it localized to the axon. In contrast, tau expressed for 1 h at 7 DIV was retained in the soma and dendrites. Our results using tau knockout neurons suggest that the reason why tau is trapped in the somatodendritic region in mature neurons is not the competition between existing endogenous tau in the axon but stable binding of tau to MTs in the soma and dendrites. PRR2_Ala showed reinforced binding presumably to MTs in FRAP and mislocalized to the soma and dendrites robustly. Interestingly, we did not detect any differences between WT and PRR2_Ala in the MT-binding assay, such that they both exhibited virtually complete and stable bindings to MTs. This is because the recombinant WT tau is completely dephosphorylated. We therefore speculate that WT tau is phosphorylated in immature neurons to reduce its MT binding, which is consistent with the faster recovery of WT tau in FRAP in the soma at 3 DIV than at 14 DIV. This notion is also consistent with the fact that tau is highly phosphorylated in the newborn brain (Watanabe et al., 1993). Furthermore, ΔMTBD was capable of localizing to the axon, even when it was expressed in mature neurons. We did confirm that ΔMTBD does not bind stably to MTs or any cytoskeletal structures in cells, evidenced by its rapid diffusional characteristics and the low level of immobile fraction in FRAP. Taken together, these results indicate that stable MT binding is surprisingly unnecessary to the axonal localization of tau. Instead, we identified PRR2 as a critical region of tau for its axonal localization. Although ΔPRR2 showed reduced MT binding like ΔMTBD, it mislocalized to the soma and dendrites even in immature neurons, unlike ΔMTBD. This again demonstrates the dissociation between MT binding and axonal localization of tau.

Potential mechanism of axonal localization

The result that highly diffusive ΔMTBD can localize to the axon prompted us to look into the mechanisms. Clearly, ΔMTBD does not localize by being trapped onto MTs or any other cytoskeletal structures in the axon. It has been proposed that a filter or barrier near the axon initial segment prevents tau from entering the soma from the axon, thereby maintaining its axonal localization (Li et al., 2011). Our results with ΔMTBD indicate that, even when axonal tau rapidly reenters the soma, the preferential axonal localization can be achieved and maintained in stage 3 neurons, in which the initial segment should not be fully established. Therefore, we conclude that at least for the initial axonal localization of tau the barrier mechanism is

---

the result observed in wild-type neurons, human tau was mislocalized to the soma and dendrites. (G) Line scan analysis of human tau (green) and MAP-2 (red) in the neuron shown in F. Top panels show high-magnification images of the area indicated in F that were used for the analysis. (H) Mislocalization of P301L tau in human tau transgenic mice in the knockout background. Even when P301L tau was expressed as a transgene in tau knockout mice, it was mislocalized to the soma and dendrites. Scale bar, 20 μm.
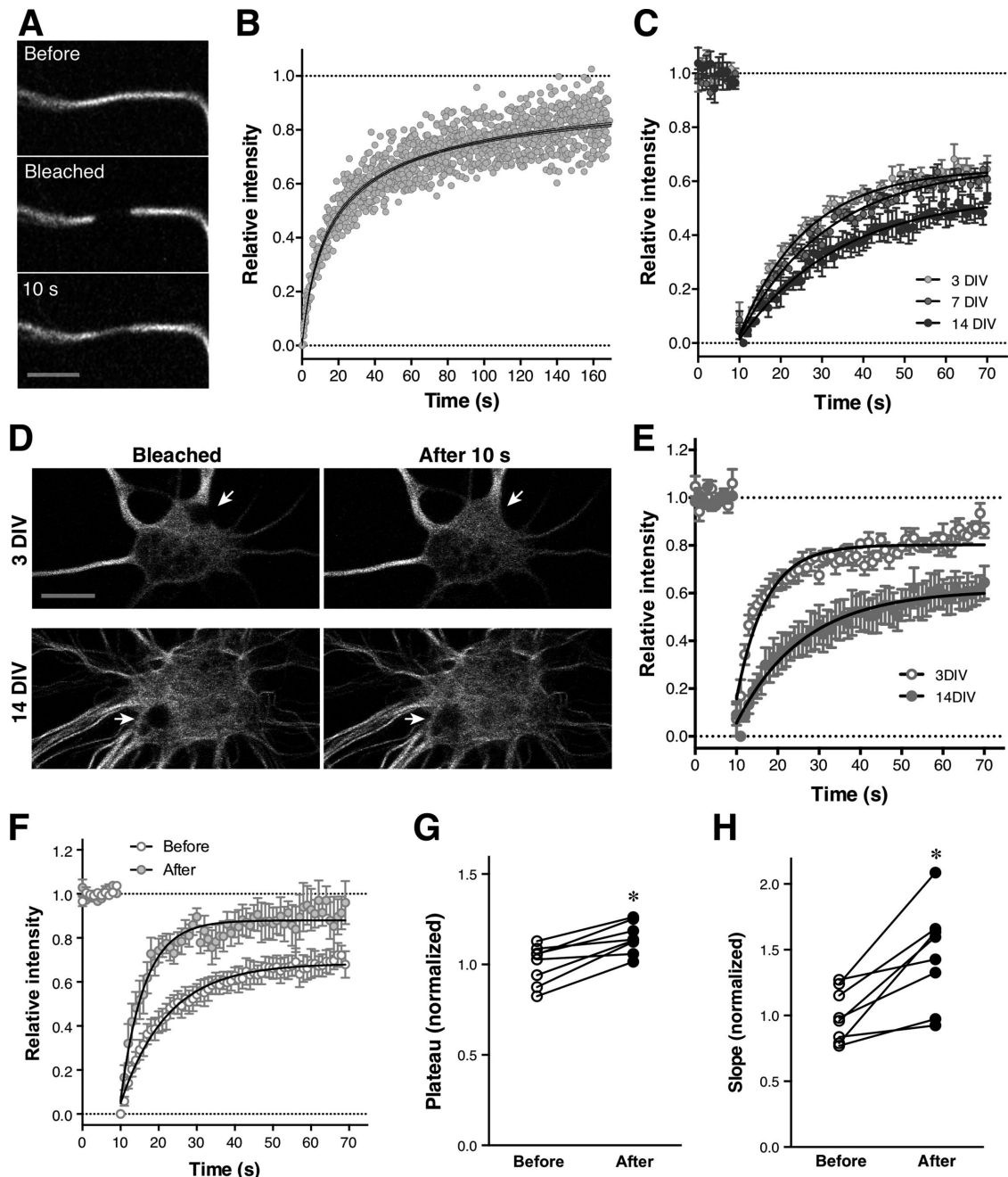
FIGURE 5: Diffusional properties of tau in neurons. (A) FRAP of GFP-tagged human tau in the axons of cultured neurons at 3 DIV. FRAP was performed in a middle portion of the axon. Images before, immediately after bleaching, and 10 s after bleaching are shown. Scale bar, 5 µm. (B) Recovery rate of fluorescence from four neurons. Individual data points are shown with gray circles. The data were fitted with a one-dimensional diffusion model with the diffusion coefficient of 0.15 ± 0.01 µm²/s, which is shown as the solid line with the 99% confidential interval (dotted lines). (C) Recovery rate of fluorescence in the axons from neurons at 3, 7, and 14 DIV. The data shown are the mean ± SEM and were fitted with exponential functions (solid lines). (D) FRAP of GFP-tagged tau in the somata of cultured neurons at 3 and 14 DIV. Images immediately after bleaching and 10 s after bleaching are shown. Arrows indicate the areas bleached. Scale bar, 10 µm. (E) Recovery rate of fluorescence in the somata. It should be noted that the somatic signals were very weak compared with those in the axon albeit detectable. The data shown are the mean ± SEM and were fitted with exponential functions. The slopes are significantly different between 3 and 14 DIV ($p < 0.0001$ with $F_{(1, 594)}$ = 32.21 using regression analysis with exponential functions). (F) FRAP of GFP-tagged tau before and after nocodazole treatment. Neurons were imaged for FRAP (Before), treated for 10–20 min with 1 µg/ml nocodazole, and reimaged (After). The data shown are the mean ± SEM and were fitted with exponential functions (solid lines). (G) Plateau values extracted from the exponential functions before and after nocodazole treatment. *, $p = 0.001$ (with $t_{(7)} = 5.422$ using a paired t test). (H) Slope values extracted from the exponential functions before and after nocodazole treatment. *, $p = 0.0039$ (with $t_{(7)} = 4.238$ using a paired t test).
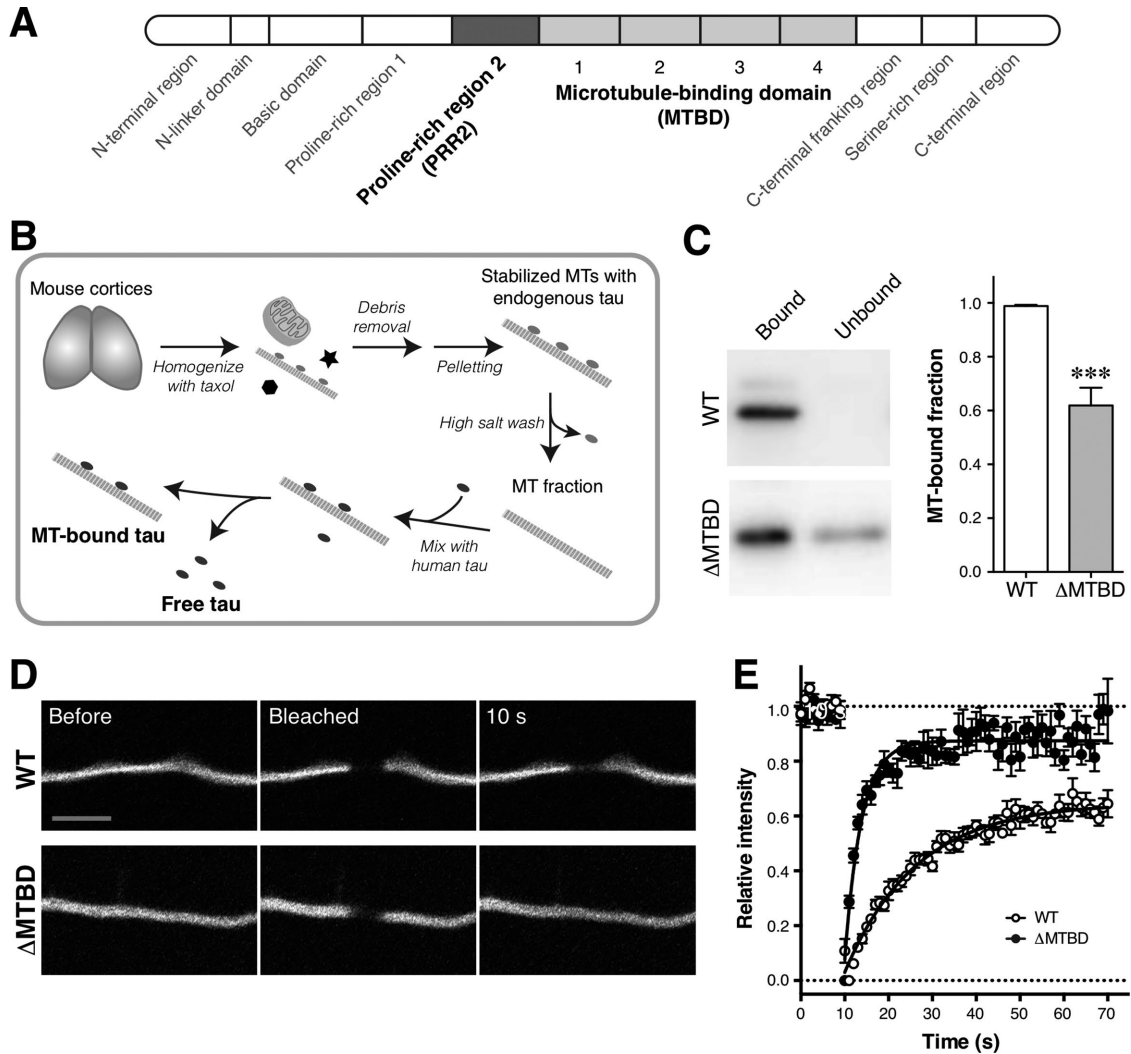
FIGURE 6: MT binding of tau in neurons. (A) Schematic diagram illustrating structural and functional domains of human tau. (B) MT-binding assay. Briefly, mouse cortices are homogenized in a warm buffer with taxol to stabilize MTs. MTs are obtained by high-speed centrifugation from the postnuclear supernatant. Bound mouse tau is removed by washing MTs with 0.5 M NaCl. This microtubule fraction is mixed with recombinant human tau for the binding assay. (C) MT binding of WT tau and tau lacking the MT-binding domain (ΔMTBD) in vitro. WT tau and ΔMTBD in MT-bound and -unbound fractions were measured using quantitative Western blotting (left panels). MT-bound fractions were normalized to the values of WT tau and shown as the mean ± SEM ($p < 0.0001$ ANOVA with Dunnett's multiple comparison test). (D) FRAP of WT tau and ΔMTBD in the axons of cultured neurons at 3 DIV. FRAP was performed in a middle portion of the axon. Images before, immediately after bleaching, and 10 s after bleaching are shown. Scale bar, 5 μm. (E) Recovery rate of fluorescence. The recovery of ΔMTBD was significantly faster than that of WT tau ($p < 0.0001$ using regression analyses).

	MT-bound	MT-unbound
WT tau	0.989 ± 0.005	0.011 ± 0.005
ΔMTBD***	0.619 ± 0.066	0.381 ± 0.066
ΔPRR2*	0.839 ± 0.012	0.161 ± 0.013
ΔPRR2-MTBD***	0.059 ± 0.017	0.941 ± 0.017
PRR2_Ala	0.993 ± 0.003	0.007 ± 0.003

Comparisons were performed using ANOVA with Dunnett's multiple comparison test. The overall difference was statistically significant ($p < 0.0001$ with $F_{(5, 30)} = 90.75$. *, $p = 0.0295$; **, $p = 0.0005$; ***, $p < 0.0001$.

TABLE 1: MT binding of tau mutants.

	Slope***	Immobile fraction***
WT tau	0.0750 ± 0.0040	0.3693 ± 0.0234
ΔMTBD	0.2833 ± 0.0262***	0.1188 ± 0.0292***
ΔPRR2	0.1389 ± 0.0157**	0.2186 ± 0.0235**
PRR2_Ala[a]	0.0112 ± 0.0020*	n.d.

[a]Because the data of PRR2_Ala could not be fitted well with a single exponential function, they were not included in the statistical analyses. Slopes and immobile fractions were analyzed using ANOVA with Dunnet post hoc comparisons to the WT tau values. The overall differences were significant at $p < 0.0001$ with $F_{(4, 25)} = 48.38$ for slope and $p < 0.0001$ with $F_{(3, 20)} = 33.12$ for the immobile fraction. Asterisks denote p values (*, $p < 0.05$; **, $p < 0.01$; and ***, $p < 0.0001$).

TABLE 2: Curve fitting parameters using exponential functions for the FRAP data.
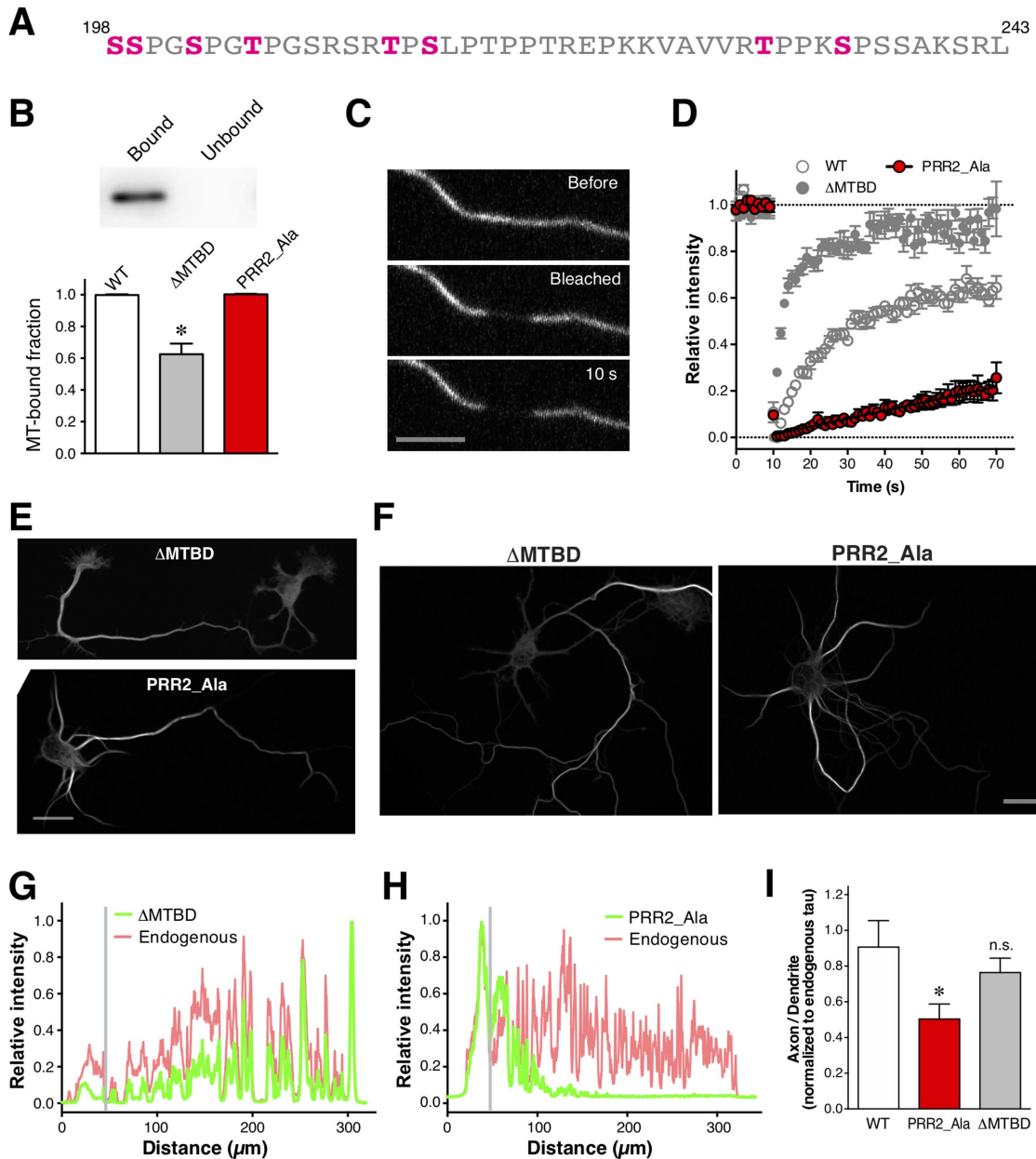
FIGURE 7: Impairment of axonal localization of tau by stable MT binding. (A) Amino acid sequence of PRR2. The bold letters indicate the eight putative phosphorylation sites mutated to Ala (PRR2_Ala). The numbering is based on the 2N4R isoform of human tau. (B) MT binding of PRR2_Ala in vitro. ΔMTBD is shown again for comparison. (C) FRAP of PRR2_Ala in the axon of a cultured neuron at 3 DIV. FRAP was performed in a middle portion of the axon. Images before, immediately after bleaching, and 10 s after bleaching are shown. Scale bar, 5 μm. (D) FRAP of PRR2_Ala in the axon of neurons at 3 DIV. Data shown are the mean ± SEM and fitted with exponential functions. Data of WT and ΔMTBD are shown in gray symbols. (E) Direct GFP signals of ΔMTBD and PRR2_Ala in neurons at 3 DIV. Scale bar, 20 μm. (F) Direct GFP signals of ΔMTBD and PRR2_Ala in neurons at 7 DIV. Scale bar, 50 μm. (G) Line scan analysis of endogenous tau (red) and ΔMTBD (green) in a 3 DIV neuron. The vertical gray lines indicate the border between the soma and the axon. (H) Line scan analysis of endogenous tau (red) and PRR2_Ala (green) in a 3 DIV neuron. The vertical gray lines indicate the border between the soma and the axon. (I) Quantification of how exogenous tau is enriched in the axon like endogenous tau using the ratio of axonal signals over dendritic signals normalized to those of endogenous tau in 3 DIV neurons. Note that a good overlap of them would provide a value close to 1. *, $p = 0.0206$ and 0.6788 for n.s. using ANOVA and Dunnett's post hoc test.

not necessary, while it is possible that a barrier helps to maintain the high axonal concentration of tau in more mature neurons.

Thus, we hypothesized that transport mechanisms continually send tau to the axon and thus work against diffusion. In fact, we observed anterogradely biased recovery with WT tau in the axonal

FRAP experiments, which indicates such directional transport. This is consistent with the fact that tau is transported by a slow axonal transport mechanism in peripheral axons and in cultured neurons (Tytell *et al.*, 1984; Mercken *et al.*, 1995; Tashiro *et al.*, 1996). Unlike the fast axonal transport, the slow axonal transport mechanisms for
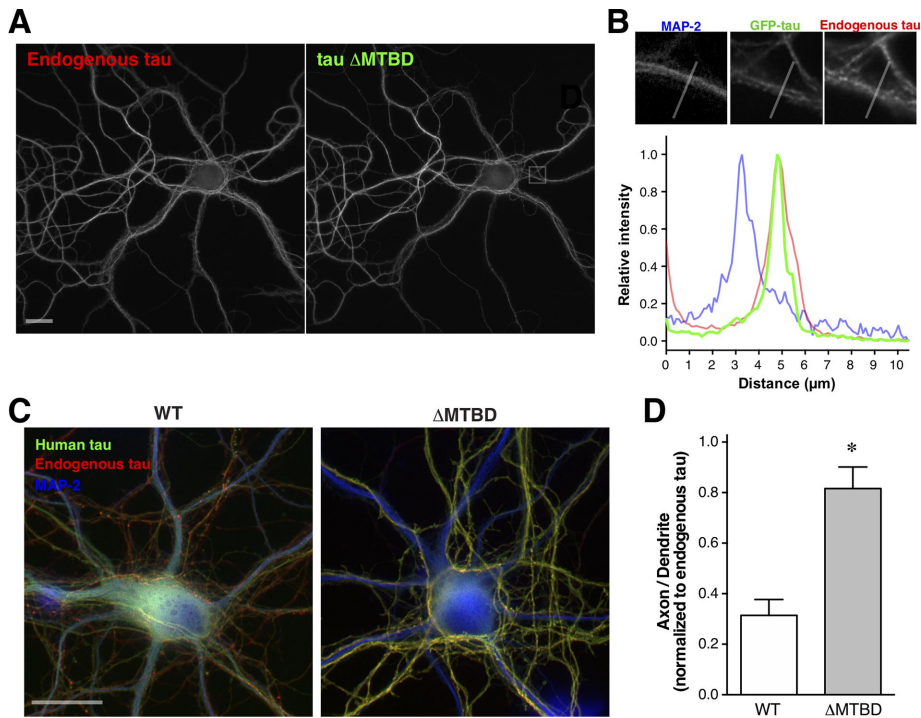
FIGURE 8: Axonal localization of tau lacking the MTBD regardless of the timing of expression. (A) Immunofluorescence labeling of endogenous tau (red, rodent tauN) and ΔMTBD (green, anti-GFP) in 14 DIV neurons, which were treated with doxycycline for the induction at 1 DIV. Scale bar, 10 μm. (B) Line scan analysis of endogenous tau (red), GFP-tau (green), and MAP-2 (blue) in the neuron shown in A. Top panels show high-magnification images of the area indicated in A that were used for the analysis. (C) Proper axonal localization of ΔMTBD but not WT tau in 14 DIV neurons, which were treated with doxycycline for the induction at 7 DIV. Scale bar, 20 μm. (D) Colocalization of ΔMTBD but not WT tau with endogenous tau in the axon. The ratio of axonal signals over dendritic signals normalized to those of endogenous tau were compared. Note that a good overlap of them would provide a value close to 1. *, $p = 0.0079$ using a Mann-Whitney test ($n = 5$).

cytosolic proteins are poorly understood (Roy, 2014). Recent studies have suggested that cytoplasmic proteins bind directly or indirectly to motor proteins and are carried by them in the axon. Because this piggybacking on the fast axonal transport is only transient and therefore short-ranged, the bulk transport of these cargo molecules appears slow. And, tau has been reported to be bound to and transported by motors (Utton *et al.*, 2005; Falzone *et al.*, 2009; Scholz and Mandelkow, 2014). Despite the rapid FRAP, the diffusivity of ΔMTBD in the axon we estimated was $2.25 \pm 0.33 \ \mu m^2/s$, which may be still low for freely diffusible proteins. Therefore, it is possible that ΔMTBD binds transiently to MTs, motors directly, or their cargoes via PRR2, and is transported toward distal axons briefly. Nevertheless, the mechanism has to be very efficient, as ΔMTBD can establish its axonal localization in immature neurons and maintain it in mature neurons.

Phosphorylation, MT binding, and axonal localization
Using FRAP to assess MT binding in cells, we confirmed that both MTBD and PRR2 participate in MT binding, with MTBD being the principal binding site (Goode *et al.*, 1997). Our results that ΔMTBD retains MT binding, presumably via PRR2, in the in vitro assay also support this idea. The deletion of PRR2 showed a modest effect on MT binding in vitro and in situ. However, the FRAP results with PRR2_Ala suggested a significant increase in MT binding, indicating that the phosphorylation state of PRR2 impacts MT binding, as previously reported (Kiris *et al.*, 2011; Schwalbe *et al.*, 2015). PRR2_Ala

mislocalized to the soma and dendrites robustly. This suggests that tight and stable binding of dephosphorylated tau prevents it from going far in the axon. Therefore, for tau to be localized in the axon, it has to be properly phosphorylated on PRR2 in the soma to benefit from the transport mechanism without being stuck on the somatic MTs. In other words, WT tau, which localizes to the axon and exhibits reduced MT binding, must be phosphorylated to some extent in neurons. Although we have not been able to identify the exact phosphorylation site(s) in PRR2 responsible for MT binding thus far, this phosphorylation of PRR2 might be the reason why our method works to localize tau to the axon. It has been shown that tau is not highly phosphorylated in mature neurons in vivo in normal conditions, whereas it is in immature neurons. Therefore, tau expressed during the developmental stages is properly phosphorylated on select sites in PRR2, not tightly bound to MTs, and efficiently transported to the axon. In fact, our data showed that WT tau in immature neurons are significantly more mobile in the soma than in mature neurons. It should also be noted that tau might undergo controlled dephosphorylation after being transported to the axon, as tau-1–positive dephosphorylated tau is highly accumulated in distal axons (Mandell and Banker, 1996). In contrast, if tau is expressed beyond the developmental period or in mature neurons, it might stay dephosphorylated, tightly binds to somatic MTs, and therefore mislocalizes to the soma and dendrites. Constitutively expressed exogenous tau would therefore be largely mislocalized to the soma and dendrites in mature neurons. Taken together, our study provides a novel experimental system for the axonal localization of tau and previously unknown MTBD-independent transport mechanisms of tau localization in neurons.

MATERIALS AND METHODS
Animals
The following animals were used in this study: Sprague Dawley rats, P301L tau–transgenic mice (P301L-Tg; Kimura *et al.*, 2010), tau knockout mice (tau-KO; Harada *et al.*, 1994; Dawson *et al.*, 2001), and tau knock-in mice (P301L-KI; Kubo *et al.*, 2019b). All animal use was approved by the institutional animal care and use committee.

Neuronal culture
Dissociated cultures of embryonic (E17–18) hippocampal neurons were prepared from female timed pregnant rats or mice (for KO mice) as previously described (Misonou *et al.*, 2008) with minor modifications. Briefly, dissected hippocampi were digested in 0.25% trypsin for 15 min at 37°C, dissociated by pipetting, and then plated onto glass coverslips coated with 1 mg/ml poly-L-lysine at 50,000 cells/coverslip. Neurons were cultured for 3–24 DIV in six-well plates, on the bottom of which contained astrocyte cultures. Coverslips were lifted with wax pedestals as described by Kaech and Banker (2006). Cytosine arabinoflanoside was added to the culture
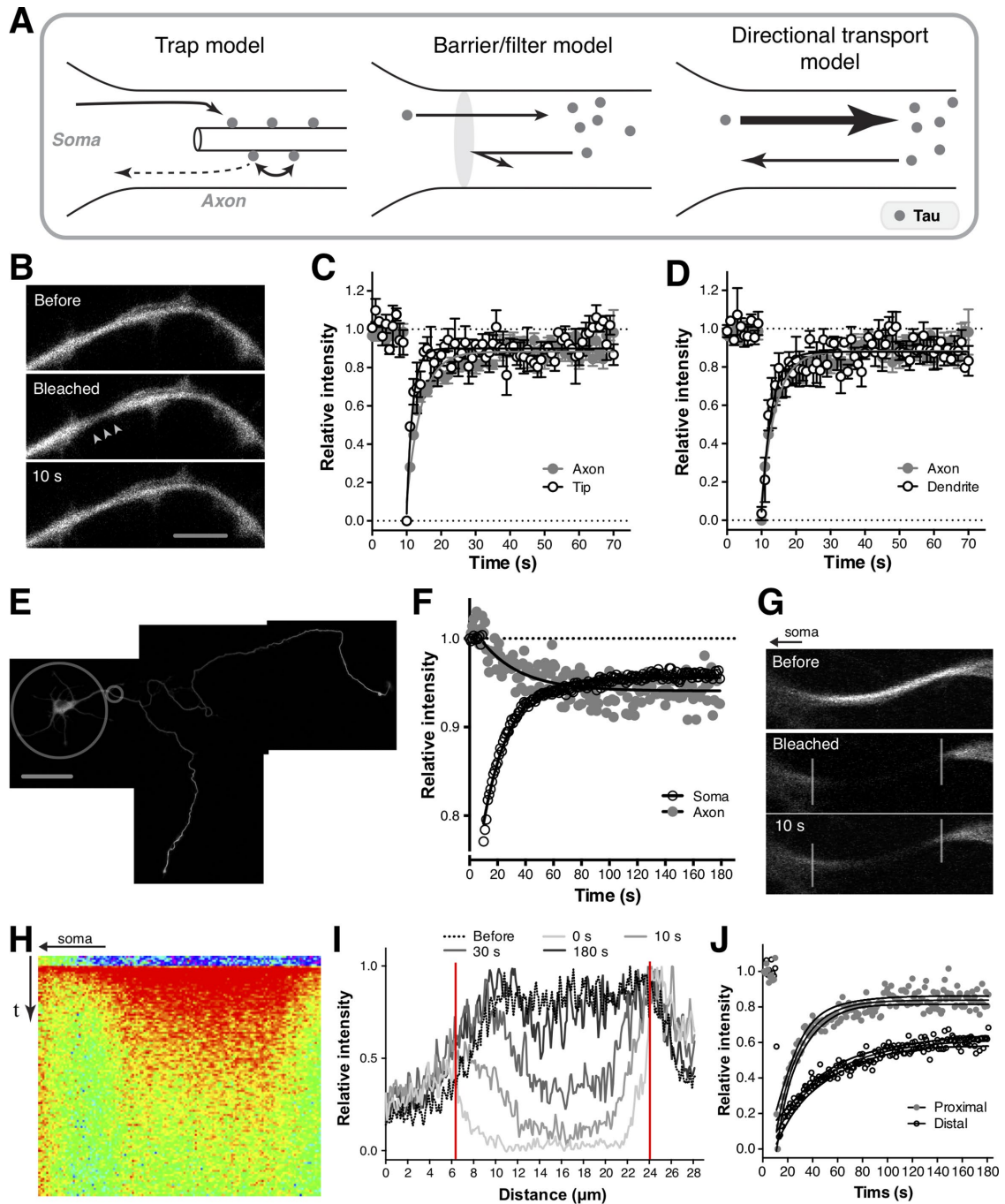
FIGURE 9: Potential mechanisms for the axonal localization of tau. (A) Three plausible models for the axonal localization of tau. The trap model assumes a stable scaffold like microtubules, which binds and traps tau (gray circles) in the axon. In the barrier/filter model, a putative barrier/filter prevents tau molecules (or complexes) from escaping from the axon, while it allows somatic tau to enter the axon. The directional transport model proposes that an active transport mechanism constitutively sends tau from the soma to the axon at a rate greater than that of tau being sent back by diffusion. (B) FRAP of ΔMTBD tau near the tip of the axon. Images before, immediately after bleaching, and 10 s after bleaching are shown. Arrowheads indicate the bleached region. Scale bar, 5 μm. (C) Rate of recovery from the experiment in B. The data shown are the mean ± SEM and those in Figure 6E are also shown for comparison. Curve fitting was done with an exponential function. The recovery was significantly faster in the tip than in the shaft of the axon ($p < 0.0001$ with $F(1, 541) = 33.46$ using regression analysis and and an F test). This is presumably due to that the tips are typically thicker than the shaft. (D) FRAP of WT tau in dendrites and axons. The data shown are the mean ± SEM and those in Figure 6E are also shown for comparison. Curve fitting was done with an exponential function. There was a slight but significant difference in the rate of recovery between dendrites and axons ($p = 0.006$ with $F(1, 601) = 7.57$ using regression analysis and an F test). This is also probably due to the larger volumes of dendrites than axons. (E) Neuron expressing ΔMTBD at 3 DIV. The large circle indicates the bleached region, and the small eclipse shows the adjacent nonbleached area in the axon used to measure the concomitant decrease of fluorescence in F. Scale bar, 50 μm. (F) Changes of fluorescence during FRAP. Open circles show the recovery in the somatodendritic region. Gray
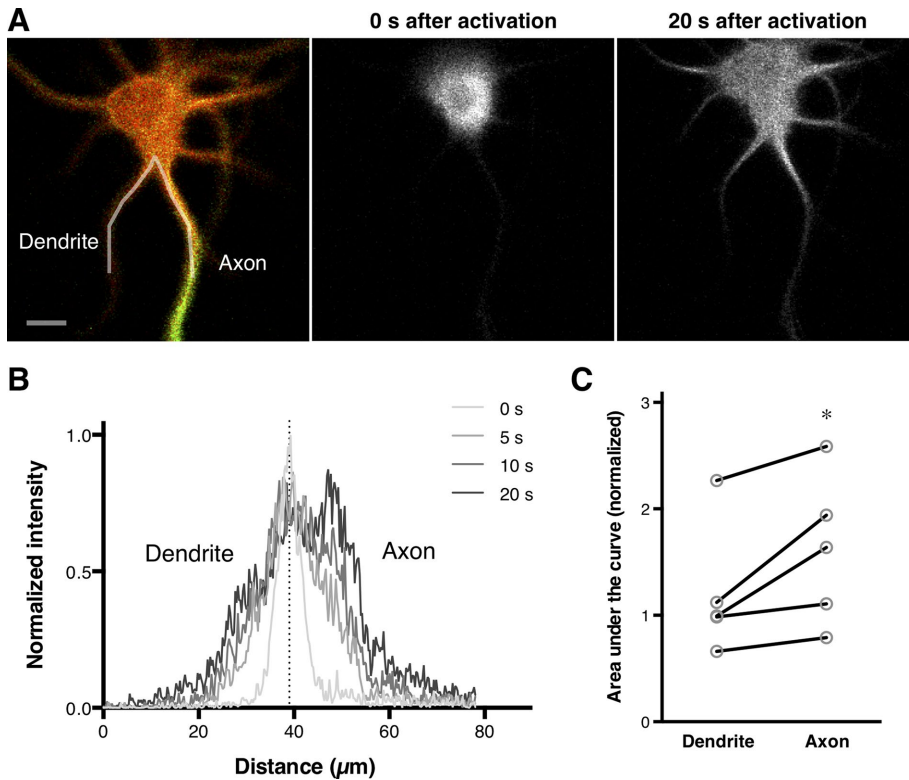
FIGURE 10: Transport of tau biased toward the axon. (A) Photoconversion of Dendra2-tagged WT tau. Expression was induced for 1 h at 1 DIV, and neurons were imaged at 3 DIV. Composite image on the left shows Dendra2-tau at 1 min after photoconversion. Gray images show immediately and 20 s after photoconversion. Scale bar, 10 μm. (B) Fluorescence intensities over the line indicated in A at different time points after photoconversion. The dotted line indicates where the profile was divided for C. (C) Area under the curve at 20 s after photoconversion. *, $p = 0.0292$ ($n = 5$).

at 2 DIV to prevent the growth of nonneuronal cells on the coverslips.

DNA constructs

Human tau cDNA corresponding to the 0N4R variant (1–383 amino acid residues) cloned into pRK172 using *Nde*I and *Eco*RI sites was generously provided by M. Goedert. For the deletion mutants, PRR2 and MTBD, corresponding regions (140–185 amino acid residues for PRR2 and 186–309 for MTBD) were removed using QuickChange mutagenesis. The coding regions of tau WT and mutants were amplified using PCR and cloned into pAcGFP (Clontech). Synthesized dephosphomimetic fragments (Eurofins Genomics) were introduced into the *Sac*II and *Pst*I sites of pAcGFP-tau. Resultant AcGFP-tau and mutants (GFP-tau hereafter) were then amplified using PCR and cloned into a pLVSIN lentiviral vector (Clontech), of which CMV promoter was replaced with the TRE3G element/promoter from pTetONE (Clontech).

Lentiviral vectors

The production of lentiviral particles was carried out as described previously (Chen and Okayama, 1987). HEK Lenti-X 293T cells were maintained in DMEM (Nacalai Tesque) with 10% fetal bovine serum (Sigma), 1 μg/ml penicillin and streptomycin in 5% CO_2 at 37°C until use. Cells were re-plated at 1×10^6 cells per 10-cm culture dish before the day of transfection. Lentiviral plasmids (6 μg of pRSV-Rev, pMD2.G, and pMDLg/p RRE plasmids from Addgene, #12253, #12259, and #12251, respectively) were mixed with 12 μg of pLVSIN containing GFP-tau and 12 μg of pRRLSIN.cPPT.PGK-GFP.WPRE (Addgene; #12252), of which EGFP was replaced with Tet3G (Clontech). The mixture was then mixed with 50 μl of 2.5 M $CaCl_2$, and supplemented with steril-ized water to adjust the volume to 500 μl. They were incubated for 20 min at room temperature (~25°C) after being mixed with 2× BES-buffered saline (50 mM BES sodium salt, 280 mM NaCl, 1.5 mM Na_2HPO_4, pH 6.95). Transfection mixture was added onto cells, which were then transferred to a 3% CO_2 incubator. The next day (after ~16–20 h), the culture medium was exchanged with 10 ml of neuronal culture medium. Transfected cells were transferred to a 5% CO_2 incubator and incubated for 2 d. Cul-ture medium was collected and filtered through a 0.45-μm filter unit into a 15- or 50-ml conical tube. Collected lentiviral solu-tion was kept at 4°C for short-term preserva-tion or at –80°C for long-term storage. For lentivirus titer measure-ment, a p-24 lenti virus titer kit (TaKaRa) was used.

Inducible expression of tau

At the day of plating, hippocampal neurons were infected with the lentivirus solution at 10–50 multiplicity of infection (MOI) overnight. Briefly, coverslips with neurons were transferred to new six-well plates with 1–1.5 ml of astrocyte conditioned media in each well. The conditioned media were prepared as described previously (Misonou and Trimmer, 2005). After the overnight incubation, the media were replaced with fresh conditioned media with 1 μg/ml doxycycline for expression induction. Coverslips were transferred back to the origi-nal six-well plates with astrocytes after 1 h induction.

Immunofluorescence labeling

Neurons were fixed in 4% paraformaldehyde/phosphate-buffered saline for 20 min. Blocking and permeabilization was done in 4%
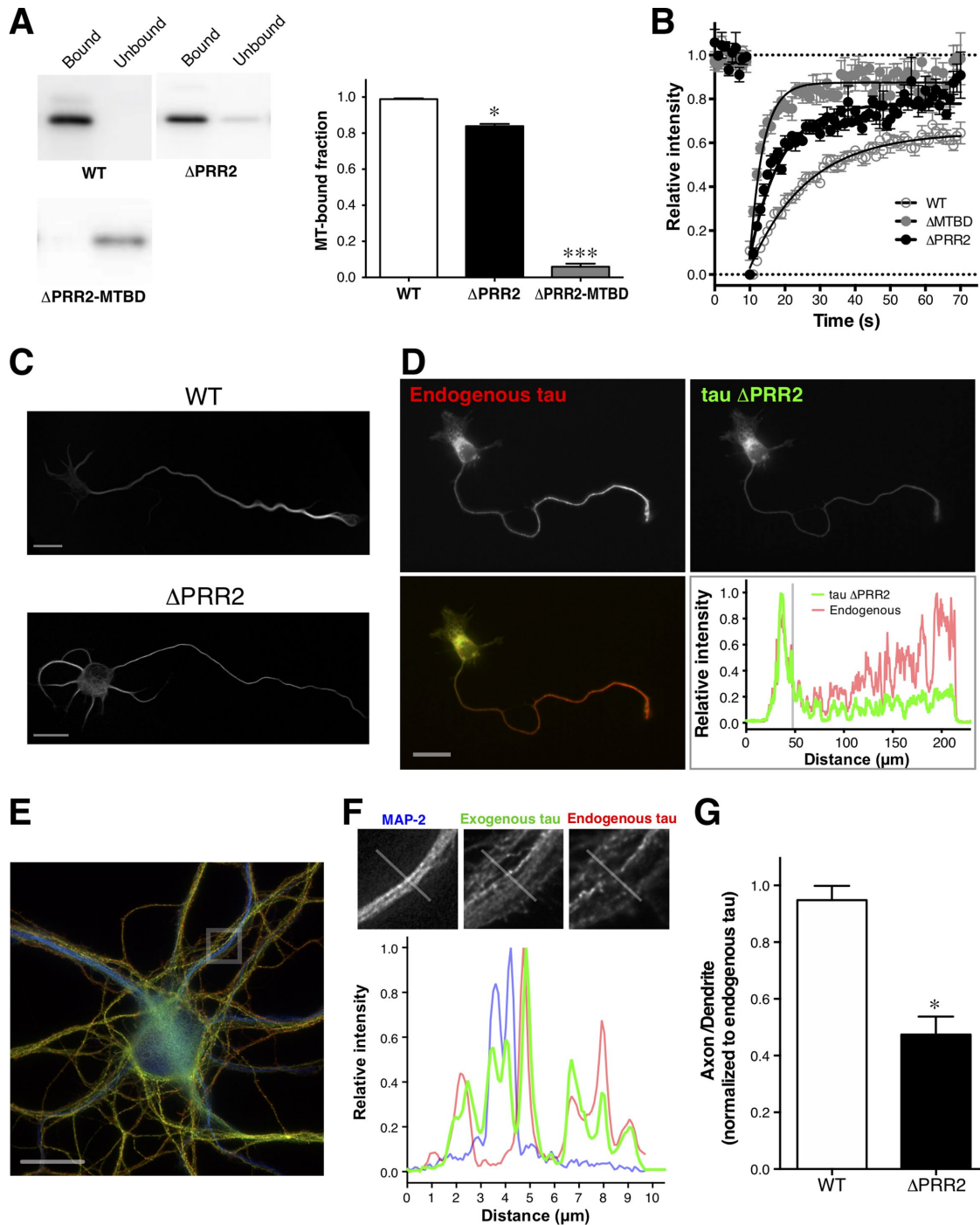
closed circles show the reduction of fluorescence in the adjacent region. It should be noted that signals were not scaled to make the minimum values zero, unlike the other FRAP plots. (G) FRAP in large areas in the proximal axon in neurons expressing WT tau. Vertical lines indicate the bleached region. Images before, immediately after bleaching, and 10 s after bleaching are shown. Scale bar, 5 μm. (H) Kymograph of the bleached region. Spectrum of color indicates the signal intensity with the longest wavelength color (red) being the lowest and the shortest wavelength color (purple) for the highest. (I) Spatial patterns of recovery. Fluorescence intensity on a line drawn over the bleached area was measured immediately and 5, 10, 30, and 180 s after bleaching, averaged in 0.5-μm bins to reduce noise, and plotted against distance. (J) FRAP at the proximal and distal ends of the bleached region. Mean values from three neurons were plotted with SEM (dotted lines).

FIGURE 11: Involvement of the PRR2 domain in the axonal localization of tau. (A) MT binding of WT tau, ΔPRR2, and tau lacking both PRR2 and MTBD (ΔPRR2-MTBD) in vitro. Tau in MT-bound fractions was measured using quantitative Western blotting (left). *, $p = 0.0295$. (B) FRAP of ΔPRR2 in the axons of 3 DIV neurons. Data from WT tau and ΔMTBD are also shown for comparison ($p < 0.0001$ vs WT tau with $F(1, 723) = 34.87$ using regression analysis). (C) Direct fluorescence images of WT tau and ΔPRR2 in neurons at 3 DIV. Scale bar, 20 μm. (D) Immunofluorescence labeling of endogenous tau (red, rodent tauN) and ΔPRR2 (green, anti-GFP) in neurons at 3 DIV. Scale bar, 20 μm. Box: Line scan analysis of endogenous tau (red) and either WT tau or ΔPRR2 (green). The vertical gray line indicates the border between the soma and the axon. (E) Triple immunolabeling of ΔPRR2 (anti-GFP), endogenous tau (rodent tauN), and MAP-2 in a 24 DIV neuron. It should be noted that there are substantial fluorescence signals of ΔPRR2 (green) in the soma. Scale bar, 20 μm. (F) Line scan analysis of endogenous tau (red), ΔPRR2 (green), and MAP-2 (blue) in the neuron shown in E. Top panels show high-magnification images of the area indicated in E that were used for the analysis. (G) Mislocalization of ΔPRR2 in mature neurons. The ratio of axonal signals over dendritic signals normalized to those of endogenous tau were compared. Note that a good overlap of them would provide a value close to 1. *, $p = 0.0079$ using a Mann-Whitney test ($n = 5$).

	Axon/dendrite ratio (normalized to endogenous tau)
WT tau	0.9069 ± 0.1478
ΔMTBD	0.7644 ± 0.0805
ΔPRR2	0.4851 ± 0.0675*
PRR2_Ala	0.5028 ± 0.0770*

Comparisons were done using ANOVA with Dunnett's post hoc tests. The overall difference was significant ($p = 0.013$ with $F (4, 28) = 3.864$). Pairwise comparisons with WT tau were performed using Dunnett's test (*, $p < 0.05$).

TABLE 3: Localization of tau mutants.

dried milk/0.1% Triton X-100/Tris-buffered saline. Primary and secondary antibodies were diluted in the same buffer and applied in separate incubation steps of 1 h and 45 min, respectively. Coverslips were mounted on glass microscope slides using ProLong Gold antifade reagent (Thermo Fisher Scientific). We used the following primary antibodies (and dilutions): rabbit anti-tau (tauN) raised against the N-term peptide (AEPRQEFEVMEDHAGGGC) of human tau, rabbit anti-rodent tau (rodent tauN) raised against the peptide (DTMEDHAGDYTLLQDEG) corresponding to the N-terminal portion of mouse tau (serum at 1:1000), rat anti-total tau (RTM38, serum at 1:5000) raised against purified recombinant human tau (Kubo *et al.*, 2019a), anti-human tau (tau12, mouse monoclonal antibody, 1:2000; Abcam), anti-GFP antibody (mouse monoclonal, 1:1000; MBL), and chicken anti-MAP2 (serum at 1:2000; Biosensis). Specificity and cross-reactivity of these antibodies to rodent and human tau have been validated (Kubo *et al.*, 2019a).

Localization analysis

The steady-state localization of tau and other marker proteins was documented using an Olympus IX73 microscope with a 60×/1.42 NA objective lens and a Andor Zyla5.5 camera, or a Carl Zeiss ApoTome system with a 63×/1.4 NA lens. A line scan analysis of fluorescence intensity was performed using ImageJ.

FRAP

Neurons expressing GFP-tagged proteins were imaged using an Olympus FV-1000 microscope or Carl Zeiss LSM 700. Images were taken every 1 s. Photobleaching was induced by applying the 450-nm laser to a circular (3.5 µm diameter) or a rectangular spot at 100% laser power for 500 ms. Fluorescence intensity was measured using ImageJ, corrected for background fluorescence and the overall bleaching due to imaging, and normalized for the maximum and minimum fluorescence intensities.

Microtubule-binding assay

Recombinant tau proteins were purified from *E. coli* transformed with pRK172 vectors encoding his-tagged human tau and deletion mutants, as previously described (Xie *et al.*, 2014). The purity was verified with SDS–PAGE and Coomassie brilliant blue staining. Microtubules were prepared as described previously with minor modifications (Miyasaka *et al.*, 2010). Briefly, mouse brains were homogenized in MT stabilization buffer (1 mM MgSO₄, 1 mM ethylene glycol-bis(β-aminoethyl ether)-N,N,N′,N′-tetraacetic acid, 0.1 mM dithiothreitol, 0.5% Triton X-100, 10% glycerol, 100 µM taxol, 2 mM GTP, protease/phosphatase inhibitors, and 0.1 M 2-ethanesulfonic acid, pH 6.8). After a brief centrifugation to remove debris, the supernatant was then centrifuged at 135,000 × *g* for 15 min at 2°C. The resultant pellet was resuspended in the MT stabilization buffer containing 0.5 M NaCl to strip endogenous tau from microtubules and centrifuged again. The pellet was resuspended in the MT stabilization buffer, and this MT fraction was used for the binding assay immediately.

Purified tau protein (250 nM as the final concentration) and 100 µl of the MT fraction were mixed and incubated on ice for 30 min. The mixture was centrifuged at 135,000 × *g* for 20 min at 2°C. The levels of tau in the supernatant (MT-unbound fraction) and in the pellet (MT-bound fraction)
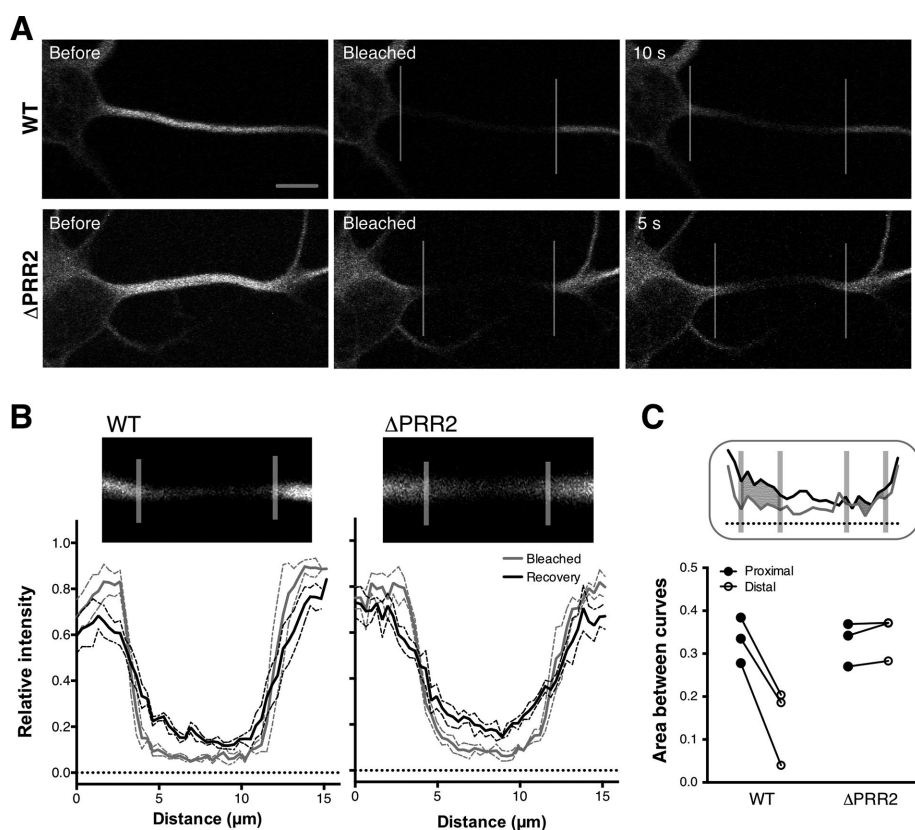

FIGURE 12: Directional transport of tau in the axon mediated by the PRR2 domain. (A) FRAP in large areas in the proximal axon in neurons expressing WT tau or ΔPRR2. Vertical lines indicate the bleached regions. Images before, immediately after bleaching, and 10 s (WT) or 5 s (ΔPRR2) after bleaching are shown. The earlier time point was chosen for ΔPRR2 because of its faster diffusion than WT (see Figure 11B). Scale bar, 5 µm. (B) Spatial patterns of recovery. Fluorescence intensity on a line drawn over the bleached area was measured immediately and 5 or 10 s after bleaching, averaged in 0.5-µm bins to reduce noise, and plotted against distance. Mean values from three neurons were plotted with SEM (dotted lines). (C) Fraction recovered was measured as the area between curves near the proximal and distal sides in the bleached area as illustrated in the inset. There is a significant difference between the proximal and distal values of WT ($p = 0.0012$ with $t (4) = 9.841$ using repeated measures two-way ANOVA with Sidak's post hoc tests) but not ΔPRR2 ($p = 0.7280$).

were quantified using Western blotting with purified recombinant tau as standards.

Experimental design and statistical analysis

All statistical analyses were performed on GraphPad Prism software (GraphPad Software, San Diego, CA). Power analysis was performed using G*Power (Faul et al., 2007, 2009) with parameters taken from previous reports or similar experiments.

FRAP data were background subtracted, compensated for bleaching from imaging, and normalized to make the minimum and maximum 0 and 1, respectively (Jensen et al., 2017). The recovery phase from the minimum was fitted with the one-phase association model: $Y = Y_0 + (\text{plateau} - Y_0) \times (1 - 10^{-k \times X})$. The difference of the fitted curves among different tau variants or in different areas in neurons was analyzed with an F test for the null hypothesis that a curve with shared parameters (slope k and plateau) fits better than those with different parameters for each data set. We also fitted data from individual neurons and obtained an averaged slope and plateau for each mutant. For Figure 3B, the recovery data were fitted with a one-dimensional diffusion model (Ellenberg and Lippincott-Schwartz, 1999) to obtain the estimate of the diffusion coefficient for WT tau.

For the analysis of axonal transport, intensity profiles over the bleached area from three neurons were obtained from right after photobleaching and 10 s (WT tau) or 5 s (ΔPRR2) later and averaged for each time point. The area between these two curves was then measured at proximal and distal areas within the bleached area and compared using a paired Student's t test.

For the MT-binding data, we normalized MT-bound fractions to those of WT tau in each experiment to compensate for the variability in MT stability. The normalized data from all tau variants were analyzed at once using ANOVA with Dunnett's post hoc tests to minimize multiple comparisons.

To compare the localization of tau mutants relative to that of endogenous tau, we measured average fluorescence intensities of expressed tau in a dendrite and the axon and computed the ratio of axonal over dendritic signals. The value was normalized to that of endogenous tau in the same neuron. We obtained normalized ratios from six to eight neurons for each tau mutant from at least two independent cultures. The averages were compared with that of WT tau using ANOVA with Dunnett's post hoc tests.

REFERENCES

Attems J, Kurt AJ (2013). Neuropathology. In: Oxford Textbook of Old Age Psychiatry, 2nd ed., ed. T Dening and A Thomas, Oxford, England: Oxford University Press.

Binder LI, Frankfurter A, Rebhun LI (1985). The distribution of tau in the mammalian central nervous system. J Cell Biol 101, 1371–1378.

Brion JP, Guilleminot J, Couchie D, Flament-Durand J, Nunez J (1988). Both adult and juvenile tau microtubule-associated proteins are axon specific in the developing and adult rat cerebellum. Neuroscience 25, 139–146.

Butner KA, Kirschner MW (1991). Tau protein binds to microtubules through a flexible array of distributed weak sites. J Cell Biol 115, 717–730.

Chen C, Okayama H (1987). High-efficiency transformation of mammalian cells by plasmid DNA. Mol Cell Biol 7, 2745–2752.

Dawson HN, Ferreira A, Eyster MV, Ghoshal N, Binder LI, Vitek MP (2001). Inhibition of neuronal maturation in primary hippocampal neurons from tau deficient mice. J Cell Sci 114, 1179–1187.

Decker JM, Krüger L, Sydow A, Zhao S, Frotscher M, Mandelkow E, Mandelkow EM (2015). Pro-aggregant Tau impairs mossy fiber plasticity due to structural changes and Ca++ dysregulation. Acta Neuropathol Commun 3, 23.

Delacourte A, David JP, Sergeant N, Buée L, Wattez A, Vermersch P, Ghozali F, Fallet-Bianco C, Pasquier F, Lebert F, et al. (1999). The biochemical pathway of neurofibrillary degeneration in aging and Alzheimer's disease. Neurology 52, 1158–1165.

Ellenberg J, Lippincott-Schwartz J (1999). Dynamics and mobility of nuclear envelope proteins in interphase and mitotic cells revealed by green fluorescent protein chimeras. Methods 19, 362–372.

Falzone TL, Stokin GB, Lillo C, Rodrigues EM, Westerman EL, Williams DS, Goldstein LS (2009). Axonal stress kinase activation and tau misbehavior induced by kinesin-1 transport defects. J Neurosci 29, 5758–5767.

Faul F, Erdfelder E, Buchner A, Lang AG (2009). Statistical power analyses using G*Power 3.1: tests for correlation and regression analyses. Behav Res Methods 41, 1149–1160.

Faul F, Erdfelder E, Lang AG, Buchner A (2007). G*Power 3: a flexible statistical power analysis program for the social, behavioral, and biomedical sciences. Behav Res Methods 39, 175–191.

Ghetti B, Oblak AL, Boeve BF, Johnson KA, Dickerson BC, Goedert M (2015). Invited review: frontotemporal dementia caused by microtubule-associated protein tau gene (MAPT) mutations: a chameleon for neuropathology and neuroimaging. Neuropathol Appl Neurobiol 41, 24–46.

Gómez-Isla T, Hollister R, West H, Mui S, Growdon JH, Petersen RC, Parisi JE, Hyman BT (1997). Neuronal loss correlates with but exceeds neurofibrillary tangles in Alzheimer's disease. Ann Neurol 41, 17–24.

Goode BL, Denis PE, Panda D, Radeke MJ, Miller HP, Wilson L, Feinstein SC (1997). Functional interactions between the proline-rich and repeat regions of tau enhance microtubule binding and assembly. Mol Biol Cell 8, 353–365.

Gustke N, Trinczek B, Biernat J, Mandelkow EM, Mandelkow E (1994). Domains of tau protein and interactions with microtubules. Biochemistry 33, 9511–9522.

Hammond JW, Huang CF, Kaech S, Jacobson C, Banker G, Verhey KJ (2010). Posttranslational modifications of tubulin and the polarized transport of kinesin-1 in neurons. Mol Biol Cell 21, 572–583.

Harada A, Oguchi K, Okabe S, Kuno J, Terada S, Ohshima T, Sato-Yoshitake R, Takei Y, Noda T, Hirokawa N (1994). Altered microtubule organization in small-calibre axons of mice lacking tau protein. Nature 369, 488–491.

Janning D, Igaev M, Sündermann F, Brühmann J, Beutel O, Heinisch JJ, Bakota L, Piehler J, Junge W, Brandt R (2014). Single-molecule tracking of tau reveals fast kiss-and-hop interaction with microtubules in living neurons. Mol Biol Cell 25, 3541–3551.

Jensen CS, Watanabe S, Stas JI, Klaphaak J, Yamane A, Schmitt N, Olesen SP, Trimmer JS, Rasmussen HB, Misonou H (2017). Trafficking of Kv2.1 Channels to the axon initial segment by a novel nonconventional secretory pathway. J Neurosci 37, 11523–11536.

Kaech S, Banker G (2006). Culturing hippocampal neurons. Nat Protoc 1, 2406–2415.

Kanai Y, Hirokawa N (1995). Sorting mechanisms of tau and MAP2 in neurons: suppressed axonal transit of MAP2 and locally regulated microtubule binding. Neuron 14, 421–432.

Kimura T, Fukuda T, Sahara N, Yamashita S, Murayama M, Mizoroki T, Yoshiike Y, Lee B, Sotiropoulos I, Maeda S, Takashima A (2010). Aggregation of detergent-insoluble tau is involved in neuronal loss but not in synaptic loss. J Biol Chem 285, 38692–38699.

Kiris E, Ventimiglia D, Sargin ME, Gaylord MR, Altinok A, Rose K, Manjunath BS, Jordan MA, Wilson L, Feinstein SC (2011). Combinatorial Tau pseudophosphorylation: markedly different regulatory effects on microtubule assembly and dynamic instability than the sum of the individual parts. J Biol Chem 286, 14257–14270.

Konzack S, Thies E, Marx A, Mandelkow EM, Mandelkow E (2007). Swimming against the tide: mobility of the microtubule-associated protein tau in neurons. J Neurosci 27, 9916–9927.

Kubo A, Misonou H, Matsuyama M, Nomori A, Wada-Kakuda S, Takashima A, Kawata M, Murayama S, Ihara Y, Miyasaka T (2019a). Distribution of endogenous normal tau in the mouse brain. J Comp Neurol 527, 985–998.

Kubo A, Ueda S, Yamane A, Wada-Kakuda S, Narita M, Matsuyama M, Nomori A, Takashima A, Kato T, Onodera O, et al. (2019b). Ectopic expression induces abnormal somatodendritic distribution of tau in the mouse brain. J Neurosci 24, 2845.

Li X, Kumar Y, Zempel H, Mandelkow EM, Biernat J, Mandelkow E (2011) Novel diffusion barrier for axonal retention of Tau in neurons and its failure in neurodegeneration. EMBO J 30, 4825–4837.

Mandell JW, Banker GA (1996). A spatial gradient of tau protein phosphory-lation in nascent axons. J Neurosci 16, 5727–5740.

Mercken M, Fischer I, Kosik KS, Nixon RA (1995). Three distinct axonal transport rates for tau, tubulin, and other microtubule-associated pro-teins: evidence for dynamic interactions of tau with microtubules in vivo. J Neurosci 15, 8259–8267.

Migheli A, Butler M, Brown K, Shelanski ML (1988). Light and electron microscope localization of the microtubule-associated tau protein in rat brain. J Neurosci 8, 1846–1851.

Misonou H, Thompson SM, Cai X (2008). Dynamic regulation of the Kv2.1 voltage-gated potassium channel during brain ischemia through neuro-glial interaction. J Neurosci 28, 8529–8538.

Misonou H, Trimmer JS (2005). A primary culture system for biochemical analyses of neuronal proteins. J Neurosci Methods 144, 165–173.

Miyasaka T, Sato S, Tatebayashi Y, Takashima A (2010). Microtubule destruc-tion induces tau liberation and its subsequent phosphorylation. FEBS Lett 584, 3227–3232.

Morales-Corraliza J, Mazzella MJ, Berger JD, Diaz NS, Choi JH, Levy E, Matsuoka Y, Planel E, Mathews PM (2009). In vivo turnover of tau and APP metabolites in the brains of wild-type and Tg2576 mice: greater stability of sAPP in the β-amyloid depositing mice. PLoS One 4, e7134.

Peng I, Binder LI, Black MM (1986). Biochemical and immunological analyses of cytoskeletal domains of neurons. J Cell Biol 102, 252–262.

Rodríguez-Martín T, Cuchillo-Ibáñez I, Noble W, Nyenya F, Anderton BH, Hanger DP (2013). Tau phosphorylation affects its axonal transport and degradation. Neurobiol Aging 34, 2146–2157.

Roy S (2014). Seeing the unseen: the hidden world of slow axonal transport. Neuroscientist 20, 71–81.

Sato C, Barthélemy NR, Mawuenyega KG, Patterson BW, Gordon BA, Jockel-Balsarotti J, Sullivan M, Crisp MJ, Kasten T, Kirmess KM, et al. (2018). Tau kinetics in neurons and the human central nervous system. Neuron 97, 1284–1298.e7.

Scholz T, Mandelkow E (2014). Transport and diffusion of Tau protein in neurons. Cell Mol Life Sci 71, 3139–3150.

Schwalbe M, Kadavath H, Biernat J, Ozenne V, Blackledge M, Mandelkow E, Zweckstetter M (2015). Structural impact of Tau phosphorylation at threonine 231. Structure 23, 1448–1458.

Song AH, Wang D, Chen G, Li Y, Luo J, Duan S, Poo MM (2009). A selective filter for cytoplasmic transport at the axon initial segment. Cell 136, 1148–1160.

Szendrei GI, Lee VM, Otvos L (1993). Recognition of the minimal epitope of monoclonal antibody Tau-1 depends upon the presence of a phosphate group but not its location. J Neurosci Res 34, 243–249.

Tashiro T, Sun X, Tsuda M, Komiya Y (1996). Differential axonal transport of soluble and insoluble tau in the rat sciatic nerve. J Neurochem 67, 1566–1574.

Tortosa E, Adolfs Y, Fukata M, Pasterkamp RJ, Kapitein LC, Hoogenraad CC (2017). Dynamic palmitoylation targets MAP6 to the axon to promote microtubule stabilization during neuronal polarization. Neuron 94, 809–825.e7.

Trojanowski JQ, Schuck T, Schmidt ML, Lee VM (1989). Distribution of tau proteins in the normal human central and peripheral nervous system. J Histochem Cytochem 37, 209–215.

Tytell M, Brady ST, Lasek RJ (1984). Axonal transport of a subclass of tau proteins: evidence for the regional differentiation of microtubules in neurons. Proc Natl Acad Sci USA 81, 1570–1574.

Urlinger S, Baron U, Thellmann M, Hasan MT, Bujard H, Hillen W (2000). Exploring the sequence space for tetracycline-dependent transcriptional activators: novel mutations yield expanded range and sensitivity. Proc Natl Acad Sci USA 97, 7963–7968.

Utton MA, Noble WJ, Hill JE, Anderton BH, Hanger DP (2005). Molecular motors implicated in the axonal transport of tau and α-synuclein. J Cell Sci 118, 4645–4654.

Watanabe A, Hasegawa M, Suzuki M, Takio K, Morishima-Kawashima M, Titani K, Arai T, Kosik KS, Ihara Y (1993). In vivo phosphorylation sites in fetal and adult rat tau. J Biol Chem 268, 25712–25717.

Weissmann C, Reyher HJ, Gauthier A, Steinhoff HJ, Junge W, Brandt R (2009). Microtubule binding and trapping at the tip of neurites regulate tau motion in living neurons. Traffic 10, 1655–1668.

Xia D, Gutmann JM, Götz J (2016). Mobility and subcellular localization of endogenous, gene-edited Tau differs from that of over-expressed human wild-type and P301L mutant Tau. Sci Rep 6, 29074.

Xie C, Miyasaka T, Yoshimura S, Hatsuta H, Yoshina S, Kage-Nakadai E, Mitani S, Murayama S, Ihara Y (2014). The homologous carboxyl-terminal domains of microtubule-associated protein 2 and TAU induce neuronal dysfunction and have differential fates in the evolution of neurofibrillary tangles. PLoS One 9, e89796.

Yamada K, Patel TK, Hochgräfe K, Mahan TE, Jiang H, Stewart FR, Mandel-kow EM, Holtzman DM (2015). Analysis of in vivo turnover of tau in a mouse model of tauopathy. Mol Neurodegener 10, 55.